

## Authors response to Reviewer 1

Comment: The paper presents and evaluates a land-surface energy flux model (SPARSE) based on the Two-Source Energy Balance (TSEB) modelling scheme. The differences between the original TSEB model and SPARSE (and their justifications) are generally well presented. However, the paper contains gaps in the description of the proposed SPARSE model (i.e. it is not clear how some of the terms were derived) and there is some confusion between the “patch” SPARSE and “parallel” TSEB implementations. Additionally, the comparison of the performance of SPARSE and original TSEB models (and therefore the evaluation of the improvements introduced by SPARSE) needs to be more robust. For example, there is no discussion of TSEB model in section 3 even though the testing of the first guess assumptions of canopy transpiring at the potential in the TSEB model (as well as in SPARSE) is listed among the main objectives of this paper in the end of section 1.

Reply: The main objective of the paper is to describe the SPARSE model and assess its limits with respect to theoretical limitations, measurements as well as simulations by a selection of published versions of TSEB. We have rephrase the sentence P4L154 in order to focus the paper on SPARSE rather than TSEB and to avoid any misunderstanding in the intended level of intercomparison with TSEB.

There are two associated grounding elements (hypotheses) in both SPARSE and TSEB models: 1- that the first guess assumption is a potential transpiration rate and 2- that if the vegetation is experiencing water stress the evaporation is at a minimum rate (null flux in general). Section 3 is mostly illustrating the limit of such assumptions in a fully synthetic and consistent framework, i.e. by using the same model in forward (“prescribed”) and inverse (“retrieval”) modes. The parameterization used by SPARSE is different from that used by TSEB, but a “prescribed” mode is clearly defined in SPARSE, contrarily to TSEB.

It is not possible to use a combination of SPARSE and TSEB in Section 3, as suggested below, because it would not be possible to interpret the results, i.e. to warranty that inconsistencies are due to the limit of the underlying assumptions and not the parameterization differences between SPARSE and TSEB. A prescribed mode could be built on the basis of TSEB, but it is beyond the scope of the study.

In Section 3, we mostly explain why the retrieval using the two core/grounding hypotheses is sometimes deficient, illustrate it with a synthetic case, and find out that for this particular case the retrieval with the parallel version is less robust. This is consistent with findings by Li et al. 2005 and Morillas et al. 2008 (see below) but brings a new light on the source of the lack of robustness for the parallel model.

The following sentence has been included P13L468: “This test has been carried out using SPARSE due to the possibility the model offers to combine both modes in a consistent synthetic experiment. Its outcomes are illustrated for this model and a single set of vegetation and climatic conditions. We don’t claim that the differences between series and parallel retrieval capacities also fully apply to TSEB but since they share the same strong underlying assumptions and differ mostly by the parameterization of the fluxes, we’re convinced that similar differences would be found with TSEB if TSEB could be run in a prescribed mode.”

Comment: Additionally, in section 4.2 only one statistical parameter (root mean square error) is used in the evaluation, the implementation details and parameterization of the TSEB model are not presented and the discussion is brief and does not always reflect the results presented in figures and tables.

Reply:

Again, the TSEB model implementation is not the core of the paper but is rather an additional estimate of the energy balance components from a related model, to compare SPARSE's outputs to. Parameterization of TSEB is that of the publications referred to, with default values of the parameters, otherwise the same inputs are used for both TSEB and SPARSE. Since both models are uncalibrated, raw performances and subsequent comparisons should be treated with care, we draw main tendencies rather than absolute rankings of both models. The fact that both model applications are done with "default" (uncalibrated) parameters is emphasized in the revised manuscript P17L617-620.

Specific comments:

Comment: P7129 L27: Series model is more robust in case of SPARES but not in case of TSEB so this statement should be more precise.

Reply: Yes, modified ("SPARSE" mentioned).

Comment: P7130 L2: Should "globally" be "generally"?

Reply: Yes, modified.

Comment: P7131 L11-12: Dual source energy balance models allow deriving of both composite and component (vegetation and soil) water stress, not just the latter.

Reply: Sentence "They also provide an estimate of the climate-controlled and moisture-limited soil evaporation rates." inserted P2L74.

Comment: P7131 L15-16: Even though there is currently no operational satellite with dual-view land surface temperature (LST) observations, the soon to be launched Sentinel-3 mission will have such capability (Donlon et al., 2012). This might be worth mentioning.

Reply: Yes, sentence inserted P3L79.

Comment: P7132 L18-19: Provide reference for the study which introduced incremental decrease of transpiration efficiency. Also what does bulk retrieval mean in this context?

Reply: The iterative procedure is mentioned along the net radiation improvement in Kustas et al. 1999 and is initially a way to solve for the unknowns  $T_s$  and  $T_c$  iteratively (Page 27: "Therefore an iteration procedure will compute LEC values below estimates given by Eq. (A.19) until values of  $T_c$  and  $T_s$  used in Eq. (A.1) agree with the measured  $TR(\zeta)$ "). The respective sentence is modified to link both improvements.

The following sentence in brackets ("bulk retrieval") is unnecessary and has been suppressed.

Comment: P7133 L2-3: It should be made more clear “classical resistance scheme” refers to Penman-Monteith formulation and that this formulation (as well as Priestley-Taylor equation) are used just to obtain the first guess of plant transpiration.

Reply: Yes, modified as suggested.

Comment: P7134 L1-3: I am not sure how T can be above the potential level since it is initially assumed to be at potential level and later can be reduced if the model doesn't obtain plausible results (i.e.  $E < 0$ ) but is never increased.

Reply: It can be above the potential level when there is a strong “micro-oasis” effect. The following sentence has been included P4L144: “Indeed, transpiration can be above its potential level when there is a strong coupling between the soil and the vegetation through conditions at aerodynamic level (stability correction notably): maximum transpiration for a plant surrounded by very dry bare soil is increased above the potential transpiration rate as computed in a fully wet environment. This coupling might be excessive and a potential transpiration of a wet environment is an interesting baseline to assess excess in this coupling.”

Comment: P7134 L15-16: The first guess assumptions of the TSEB model are not tested in this study since section 3 deals only with SPARSE model. It would be interesting to evaluate the performance of the original TSEB formulations in retrieving the transpiration and evaporation efficiencies. Possibly it could be done by running SPARSE in prescribed mode, then using the resulting temperature as input to TSEB model and estimating the efficiencies by dividing  $LE_s$  and  $LE_v$  by their respective potential values.

Reply: This could be interesting, but then it would not be possible to evaluate whether retrieved efficiencies (simulated using a combination of SPARSE and TSEB) are different to the prescribed ones (simulated by SPARSE) because of the differences between SPARSE and TSEB, or only due to the TSEB algorithm.

Comment: P7134 L21 – P7135 L2: It would be more clear if the order of the equations presented here corresponded to the order in which those equations are introduced in sections 2.1.1 and 2.1.2 and mentioned on P7144 L5-6 (i.e. latent heat flux equations, followed by energy budget of soil and vegetation and finally relating radiative surface temperature to the temperatures of soil and vegetation).

Reply: Agreed, this has been changed accordingly.

Comment: P7137 L15-16: More details of the iterative procedure should be given. This is its only mention in the whole manuscript.

Reply: This is an alternative version only, its mention has been suppressed for the sake of clarity.

Comment: P7139 L17: How is  $R_{atm}$  obtained in this study? Was it measured (there is no mention of that in section 4.1), estimated from  $T_a$  or obtained in another way?

Reply:  $R_{atm}$  was estimated from  $T_a$  (Brutsaert clear sky  $R_{atm}$  equation provided P23L842).

Comment: P7140 L4:  $T_{\text{rad}}$  is often observed from angles other than nadir and becomes  $T_{\text{rad}}(\theta)$  where  $\theta$  is the view zenith angle. How is the view zenith angle accounted for in eq. 17? In appendix A2 there is a vegetation cover fraction ( $f_c$ ) parameter but there is no explanation of how it is derived and I couldn't see any parameter taking  $\theta$  into account.

Reply: Equation provided P23L841, also it is specified that we use data acquired at nadir (P13L482).

Comment: P7141 L5-L9: Why are the stability correction factors not estimated separately if  $T_{0s}$  and  $T_{0v}$  are known?

Reply: This is explained P7131 L28-P7132 L12: vegetation and soil patches are linked, linked in TSEB, only though their common stability conditions with a common Surface Boundary Layer.

Comment: In appendix A1  $z_{om,s}$  is already estimated and  $d$  could also be estimated thus  $r_{a,s}$  and Richardson number could also be estimated separately for soil and vegetation. What would be the expected effect of estimating  $r_{a,s}$  and  $r_{a,v}$  separately?

Reply: Again, cf. P7131 L28-P7132 L12: this would mean that there are two SBLs above the soil and the vegetation, which, given the size of the respective areas, is not realistic.

Comment: P7141 L12: Again, how is  $f_c$  estimated.

Reply: cf supra.

Comment: P7141 L15-18: The "patch" representation of SPARSE model consists of two independent flux networks (one for vegetation and one for soil) which are combined using the fraction of sub-pixel the source of each flux occupies. In this approach the fluxes represent current densities if the resistance networks are considered in electrical terms (Sanchez et al. 2008). In the "parallel" TSEB implementation the interaction between the canopy and soil fluxes is still minimal but the two component fluxes are added up to obtain the total flux. This implies that the fluxes are treated as currents in electronic networks since currents are additive when two parallel branches meet. Therefore, even though both approaches ("patch" and "parallel") are correct based on the assumption they make, they are not directly comparable and the interchangeable use of "patch" and "parallel" terms when describing SPARSE might be confusing when the "parallel" TSEB term is also used in the manuscript. Therefore the difference between the two approaches should be clearly described and taken into account when analysing TSEB and SPARSE model results.

Reply: The differences between the translations of the "patch approach" into the parallel algorithm of TSEB and other formalisms have been detailed in Lhomme and Chehbouni (1999) and re-assessed in Lhomme et al. (2012) who refer to the latter earlier comment. The way the total turbulent heat fluxes are computed from the soil and vegetation components is not very different in fine between both models: in TSEB, each component flux ( $H_s$  or  $H_v$ ) is directly expressed for the whole surface once the available energy has been partitioned into a soil and a vegetation patch according to  $f_c$ , therefore the total flux is the simple arithmetic sum of both (Equation 7 of Norman et al. 1995). In SPARSE, we describe each flux density of each patch, i.e. one for the soil and one for the vegetation. Therefore the partitioning is computed once the individual flux is computed after solving the surface energy balance for each patch, and the total is therefore computed as a weighted sum and no longer

a simple sum. It seems to us that this choice is more consistent with the “patch approach” defined by Lhomme et al. (2012) and schematized in Figure 1

Comment: P7147 L28: In the figure the indicated efficiency is 0.6

Reply: Yes, corrected.

P7148 – Section 3: What would be the effect of incrementally reducing  $B_v$  and re- running the model in case of negative evaporation instead of setting  $B_s$  immediately to 0? You mention this technique as an improvement to original TSEB on P7132 P18-19 so why not implement it in SPARSE. Also, the performance of TSEB should also be assessed in this section (see comment related to P7134 L15-16).

Reply: In SPARSE, all variables are solved simultaneously, including  $T_s$  and  $T_v$ , therefore the iterative procedure to reduce  $B_v$  to reach convergence is not useful.

Comment: P7149 L3: Was LST acquired from nadir? If it was acquired at a different view zenith angle then how was this taken into account?

Reply: It was acquired at nadir, it's now specified P13L482.

Comment: P7149 L8: Does residual method mean that residual energy was assigned to LE or H? Also maybe consider the approach from the study of Ingwersen et al. (2015).

Reply: In this experiment, there was clearly a problem with the fast response psychrometer, but we'll keep your suggestion in mind for closure analysis in the future evaluations of SPARSE.

Comment: P7149 L18-19: In Section 4.2 it is often not clear which models are being discussed. The original TSEB model implementations should be listed here and not only in the caption of Table 1. Why are different references used for the parallel and series versions of TSEB? Cammalleri et al. (2010) were looking at different representations of wind profile in the canopy but did not present any modifications to the actual TSEB formulations. So is one of the wind profile models presented in Cammalleri et al. (2010) used in the series version of TSEB but not in the parallel? What would be the justification for that and which wind profile model was used? Also implementation and parameterization details of the TSEB model should be clearly stated. For example, what default value of  $\alpha_{PT}$  was used, was clumping factor used, was fraction of vegetation that is green ( $f_g$ ) set to 1 or varied during senescence. In particular it would be interesting to look at the effects of varying or not varying  $f_g$  estimate in the TSEB model as it has a large effect on the estimated fluxes and is available in this study since hemispherical photography and destructive sampling were used to estimate LAI.

Reply: We've used the TSEB series and parallel versions of Kustas et al., (1999), i.e. the Goudriaan (1977) wind profile. We mentioned Cammalleri et al. (2010) because it is a more recent and complete description of the series model including choices of parameter default values for the resistance  $r_{as}$ . it is therefore not necessary to refer to it if parameter values are specified and we keep the Kustas et al. 1999 reference for the model. We also specify that  $\alpha_{PT}$  was set to its classical value 1.26. Green and total LAI index are shown.

Comment: P7150 L1: If the model is designed to be routinely applied with remote sensing data then it should be explained how the view zenith angle of the LST observations is taken into account.

Reply: Yes, cf supra.

Comment: P7150 L5-6: More thorough statistical analysis should be performed and presented in Table 1 (and Table 2).

Reply: Yes, cf. supra.

Comment: The effect of bounding LE estimates should be explored by looking not only at RMSE but also other statistical parameters, for example (but not necessarily limited to) bias, correlation or coefficient of variation. During what conditions do the outputs have to be bound? Is it mainly during plant growth stage or senescence?

Reply: It is mostly important in selected dates, the following sentence has been included P15L553: "Without bounding, values of evaporation and transpiration above potential levels are obtained for the series version during vegetation growth, and some negative values of transpiration are found during late maturity and beginning of senescence".

Comment: P7150 L6-13: The description in this paragraph does not reflect the results presented in Table 1. For example, the RMSE of parallel and series versions of SPARSE are not "almost similar" as stated on L7 (see difference between non-bounded models in irrigated wheat),

Reply: We agree, but since the model is uncalibrated differences must be described with special care. We replaced change "almost similar" by "of similar order of magnitudes".

Comment: The reduction in RMSE stated on L9 is only true for SPARSE model and the statements on L9-13 are only true for bounded versions of the models. I would suggest rewriting this paragraph (after further statistical measures have been included in Table 1) and being more clear about which version of the model (SPARSE/TSEB, parallel/series, bounded/unbounded) is being discussed.

Reply: Agreed and specified accordingly.

Comment: P7150 L14-15: Are any fluxes recalculated after  $LE_s$  and  $LE_v$  are bounded? If not, then wouldn't the estimates for  $H$ ,  $G$  and  $R_n$  be the same for bounded and unbounded case?

Reply: Yes, the following sentence is added: "For consistency, if  $LE_x$  is limited by  $LE_x(\beta_s=1, \beta_v=1)$ , all fluxes of the corresponding component energy balance ( $R_{n_x}$ ,  $H_x$  and  $G$ ) are set to their values obtained by the "prescribed" mode in potential conditions, i.e.  $R_{n_x}(\beta_s=1, \beta_v=1)$ ,  $H_x(\beta_s=1, \beta_v=1)$  and  $G(\beta_s=1, \beta_v=1)$ ."

Comment: P7150 L18: Be more clear in what exactly is consistent with Li et al. (2005) and Morillas et al. (2013). What did those studies show?

Reply: Those studies indicate that the series model tend to provide more robust and slightly better results, but that the parallel model does not always show significantly worse statistical criteria. This will be made explicit.

Comment: P7151 L20-23: On L20, should it be “little to no stress” instead of “little to no evaporation”? Furthermore in top-right Figure 3 (low evaporation efficiency) the most accurate retrieval of evapotranspiration efficiency for parallel SPARSE model is for high transpiration efficiencies (small vegetation stress values) which is contradictory with the statement on L22-23.

Reply: We're referring to evaporation only, it has been specified.

Comment: P7152 L14: How is  $\theta_{sat}$  estimated and what is its value?

Reply: It is obtained in-situ (values given).

Comment: P7153 L5-9: Can the temporal pattern of agreement be explained by the patch/layer representations present in parallel/series SPARSE model versions being more appropriate at different stages of vegetation development?

Reply: It was not possible to relate those patterns for sure to specificities of both model representations.

Comment: P7154 L3-5: Was this finding presented in the results section? P7154 L5-6: I do not understand this sentence.

Reply: This refers to section 3 findings only (it has been specified).

Comment: P7154 L17: It should be 0.2 not 0.1.

Reply: Agreed and changed accordingly.

Comment: P7154 L27-28: In the rainfed field senescence began around DOY 80 and vegetation was fully brown by around DOY 120 (Fig 3). Looking at Fig 10 the agreement between the soil evaporation efficiencies modelled with SPARSE and soil moisture data agree very well between DOY 120 and DOY 160. Therefore, at least at this site SPARSE models seems to be performing well over “low or senescent vegetation” (although between DOY 80 and DOY 120 the agreement is not so good). This is not fully consistent with statement on L27-28.

Reply: As pointed out, there is a mismatch between observed and simulated soil efficiencies before DOY120 and after DOY160, on the basis of which this general comment is drawn. However, the good performance between DOY 120 and DOY160 is mentioned P7153 L7. On that basis the previous statement is softened in P7154 L28-29.

Comment: P7156 L4-5: How are  $d$  and  $z_{om}$  estimated?

Reply: Equations provided P23L826.

Comment: Table 1: Add more statistical measures as mentioned in comment P7150 L5-6.

Reply: Done (MAPE and correlation provided).

Comment: Table 2: Add more statistical measures to be consistent with Table 1. Also, why was the series TSEB model not included in this table?

Reply: Done (MAPE and correlation provided).

Comment: Table A1: There are some mistakes present in this table. For example  $r_a$ ,  $r_{as}$ ,  $r_{av}$  and  $r_w$  have the same definition. Double check the other parameters as well.

Reply: Yes, corrected.

Comment: Figure 2: This figure is too complicated. I would remove the input data for synthetic test and also the synthetic test branch (broken line) to improve clarity.

Reply: This line is useful for section 3, but has been dropped.

Comment: Figure 5: The shown plots appear to be for green LAI. It would be good to also show total LAI and possibly  $f_g$ , especially if the effect of varying  $f_g$  in the TSEB model during senescence is investigated as suggested in comment P7149 L18-19.

Reply: Done

Comment: Figures 7 and 9: The legend captions should be fixed.

Reply: Corrected.



## Authors response to Reviewer 2

Comment:

Page 12 Eq. (7) & (8): How are  $T_s$  and  $T_v$  determined and is the view angle of the radiometer accommodated? I can't find an expression in the text that describes this.

Reply: In order to improve the clarity of the model's description, we have added explicitly the symbols  $T_s$  and  $T_v$  in the model's introduction to stress that it is derived by solving the system of equations (beginning of section 2.1).

Information about the radiometer view-angle (nadir, P13L482) and an equation to use  $Trad$  from a different view angle (this is also suggested by Reviewer 1) following the view angle dependent vegetation fraction cover have been added (P23L841).

Comment:

Page 15 Eq. (24): What is the physical basis for simply weighting the aerodynamic temperature estimated for the soil and vegetation? In addition, have two aerodynamic temperatures for the soil-canopy system is not physically plausible at the canopy/micrometeorological scale-this needs some explanation/discussion.

Reply: This section has been rewritten and is now: "For the parallel model, the sensible heat flux rate above each patch is:

$$H_s = \rho c_p \frac{T_s - T_a}{r_{as} + r_a} \quad (22)$$

for the soil, and

$$H_v = \rho c_p \frac{T_v - T_a}{r_{av} + r_a} \quad (23)$$

for the vegetation.

The value of the Leaf Area Index used for the parallel model is a "clump LAI" obtained by dividing the total LAI by the fraction cover of the vegetation  $f_c$  (Lhomme and Chehbouni, 1999). Total fluxes are the sum of the soil and vegetation components also weighted by their relative contribution,  $f_c$  for the vegetation and  $1-f_c$  for the soil:

$$LE = (1 - f_c)LE_s + f_cLE_v \quad (24)$$

where  $LE_s$  is expressed according to (20) and  $LE_v$  to (21), and

$$H = (1 - f_c)H_s + f_cH_v \quad (25)$$

where  $H_s$  is expressed according to (22) and  $H_v$  to (23).

The stability correction for the aerodynamic resistance  $r_a$  depends on an average aerodynamic temperature computed from the total sensible heat flux  $H$ :

$$T_0 = T_a + \frac{Hr_a}{\rho c_p} "$$

Comment:

Page 17 Lines 5-9. It's unclear to me how the iterative procedure works more clarification is needed.

Reply: This alternative way of solving the system of equations is not necessary and has been removed.

Comment:

Page 18 Lines 21-24. The discussion of realistic bounds for  $LE_x$  based on Su (2002) seems to be a critical part of the modeling approach, but is not explained in any detail. Some further discussion is needed.

The paragraph has been rewritten: "Finally, in order to ensure that  $LE_x$  outputs are within realistic bounds,  $LE_x$  values obtained by running SPARSE in "retrieval" conditions are limited by the evapotranspiration components in potential conditions  $LE_x(\beta_s=1, \beta_v=1)$  computed by SPARSE in prescribed potential conditions (Figure2). This procedure is the dual source equivalent of what is done in the single-source model SEBS (Su, 2002)."

Comment:

Page 19 Section 3.1/3.2. It's not clear to me if this simulation experiment/synthetic test is truly independent of the model structure. Why didn't the authors use a more complex SVAT that generates Trad, Ts and Tv and component fluxes to compare with SPARSE? Justification for this synthetic test needs to be made.

Reply: The synthetic test illustrates the theoretical limit of the 2 underlying assumptions of SPARSE, which are also the underlying assumptions of most TSEB versions. It builds on the existence of both modes (prescribed and retrieval) of SPARSE to test the capacity of the model to retrieve correctly the water status of both sources (represented in SPARSE by their respective efficiencies) when they are known. It is important to keep the same model and the same parameters for this test, because otherwise it would be impossible to know whether inconsistencies between the prescribed and the retrieved efficiencies are due to the model structure or represent the theoretical limit of the retrieval (absence of bijective relationships) due to its assumptions. The following sentences have been added:

P4L157: "The purpose of the simulation experiment is specifically to test the limits of the underlying first guess assumptions of SPARSE, which are identical to those used in most TSEB versions."

P13L468: "This test has been carried out using SPARSE due to the possibility the model offers to combine both modes in a consistent synthetic experiment. Its outcomes are illustrated for this model and a single set of vegetation and climatic conditions. We don't claim that the differences between series and parallel retrieval capacities also fully apply to TSEB but since they share the same strong underlying assumptions and differ mostly by their parameterization of the fluxes, we're convinced that similar differences would be found with TSEB if TSEB could be run in a prescribed mode."

Comment:

Page 23 Line 5. What was the closure values achieved by the eddy covariance system and what was done with the missing energy flux?

The following sentences are inserted P13L484: “For the rainfed wheat site, there was clearly a problem with the fast response psychrometer with an energy balance closure of 60 %. Thus for that site the closure was forced and the corrected LE was computed as  $R_n - H - G$ . For the irrigated site, the half hourly closure was of the order of 80%. For this site closure was achieved with the conservation of the Bowen ratio  $H/LE$ , thus the corrected LE was computed as  $(R_n - G)/(1 + H/LE)$ .”

Page 23 Lines 26-27. The minimum stomatal resistance was set to 100 s/m, so what would happen if 50 m/s was chosen? This is certainly plausible for cereal crops.

The following sentence has been inserted P17L619: “If a value of  $r_{stmin} = 50$  s/m is used, a value also reported for wheat crops in more temperate regions, RMSE on latent heat flux increases by 4 W/m<sup>2</sup> in bounded conditions for the rainfed wheat site (62 W/m<sup>2</sup>) and 13 W/m<sup>2</sup> for the irrigated wheat site (66 W/m<sup>2</sup>) for the series version. For the parallel model it increases by 12 W/m<sup>2</sup> (82 W/m<sup>2</sup>) and 8 W/m<sup>2</sup> (74 W/m<sup>2</sup>), respectively.”

Comment:

Page 24 Lines 5-19. There is little explanation again on how the bounded versus unbounded model results were determined.

Reply: cf. supra.

Comment:

Also Tables 1 and 2 should include more statistics, such as mean of observed and modeled, also the mean absolute error statistic and a percentage difference.

Reply:

MAPE and correlation coefficient have added in both Tables, as requested by both Reviewer 1 and 2. Mean of observed and modeled fluxes are useful in the case of applications to individual surface temperature images, but represent a wide range of situations over the whole season, it would be difficult to extract additional information from these values if biases are mentioned.

Comment:

Moreover, I'm confused that the series TSEB model is based on a citation from Cammalleri et al (2010) while the authors use the citation for TSEB parallel version of Kustas and Norman (1999), even though I believe a series version is also developed in that paper. There needs to be an explanation as to what the differences are in TSEB formulations used in the 2 papers.

We now mention that in TSEB is run with a nominal (1.26) value for the PT coefficient (see also the Reply to Reveiwer 1 comments) and use the single reference Kustas et al., 1999 for both model versions.

Comment:

Page 28 Lines 5-8. So is the SPARSE model considered more reliable than the TSEB based on Table 1 and 2 results?

TSEB and SPARSE are run with default values corresponding to typical vegetation classes, as it is the case for routine applications of remote sensing energy balance models to lead to spatially distributed

evapotranspiration products. They were not calibrated against in-situ data. It is thus difficult to conclude on their absolute respective reliability. We compare their relative performance with default values on 2 datasets only. We do not claim that SPARSE is more reliable than TSEB, but find that SPARSE with default values of the parameters performs better TSEB for those 2 datasets. The following sentence has been inserted P17L617: "This comparison must be treated with special care since both models are run with no prior calibration of the poorly known parameters such as the minimum stomatal resistance (for SPARSE) or the Priestly-Taylor coefficient (for TSEB)".

Comment:

In larger scale applications, should the authors consider a lack of having reliable vapor pressure data and what impact this may have on models such as SPARSE which require this input?

Reply: The final sentence has been added: "SPARSE needs more input data than TSEB, for instance relative humidity. The impact of uncertainty on available meteorological data (reanalysis or remote-sensing meteorological products vs local meteorological stations network) on SPARSE model performance will also be assessed in the future."

**Marked-up MS version:**

1 **The SPARSE model for the prediction of water stress and evapotranspiration**  
2 **components from thermal infra-red data and its evaluation over irrigated and**  
3 **rainfed wheat.**

4

5 G. Boulet<sup>\*1,2</sup>, B. Mougenot<sup>1,2</sup>, J.-P. Lhomme<sup>3</sup>, P. Fanise<sup>1</sup>, Z. Lili-Chabaane<sup>2</sup>, A. Olioso<sup>4,5</sup>, M. Bahir<sup>1,4,5</sup>, V.  
6 Rivalland<sup>1</sup>, L. Jarlan<sup>1</sup>, O. Merlin<sup>1</sup>, B. Coudert<sup>1</sup>, S. Er-Raki<sup>6</sup> and J.-P. Lagouarde<sup>7</sup>

7 <sup>1</sup> CESBIO - UMR 5126 UPS, CNRS, CNES, IRD, Toulouse, France

8 <sup>2</sup> Département Génie Rural des Eaux et Forêts, Institut National Agronomique de Tunisie Université de  
9 Carthage, Tunis, Tunisia

10 <sup>3</sup> IRD, UMR LISAH, Montpellier, France

11 <sup>4</sup> INRA, EMMAH – UMR1114, Avignon, France

12 <sup>5</sup> UAPV, EMMAH – UMR1114, Avignon, France

13 <sup>6</sup> LP2M2E, FST, Université Cadi Ayyad, Marrakech, Morocco

14 <sup>7</sup> INRA, UMR 1391 ISPA, 33140 Villenave d'Ornon, France

15 \* [Gilles.Boulet@ird.fr](mailto:Gilles.Boulet@ird.fr)

16

17 **Abstract**

18 Evapotranspiration is an important component of the water cycle, especially in semi-arid lands. A way  
19 to quantify the spatial distribution of evapotranspiration and water stress from remote-sensing data  
20 is to exploit the available surface temperature as a signature of the surface energy balance. Remotely  
21 sensed energy balance models enable to estimate stress levels and, in turn, the water status of  
22 continental surfaces. Dual-source models are particularly useful since they allow deriving a rough  
23 estimate of the water stress of the vegetation instead of that of a soil-vegetation composite. They  
24 either assume that the soil and the vegetation interact almost independently with the atmosphere  
25 (patch approach corresponding to a parallel resistance scheme) or are tightly coupled (layer approach  
26 corresponding to a series resistance scheme). The water status of both sources is solved  
27 simultaneously from a single surface temperature observation based on a realistic underlying  
28 assumption which states that, in most cases, the vegetation is unstressed, and that if the vegetation is  
29 stressed, evaporation is negligible. In the latter case, if the vegetation stress is not properly accounted  
30 for, the resulting evaporation will decrease to unrealistic levels (negative fluxes) in order to maintain  
31 the same total surface temperature. This work assesses the retrieval performances of total and  
32 component evapotranspiration as well as surface and plant water stress levels by 1- proposing a new  
33 dual-source model named Soil Plant Atmosphere and Remote Sensing Evapotranspiration (SPARSE) in  
34 two versions (parallel and series resistance networks) based on the TSEB (Norman et al., 1995) model  
35 rationale as well as state of the art formulations of turbulent and radiative exchange, 2- challenging

36 the limits of the underlying hypothesis for those two versions through a synthetic retrieval test and 3-  
37 testing the water stress retrievals (vegetation water stress and moisture-limited soil evaporation)  
38 against in-situ data over contrasted test sites (irrigated and rainfed wheat). We demonstrated with  
39 those two datasets that the [SPARSE](#) series model is more robust to component stress retrieval for this  
40 cover type, that its performance increases by using bounding relationships based on potential  
41 conditions (Root Mean Square Error lowered by up to 11 W/m<sup>2</sup> from values of the order of 50-80  
42 W/m<sup>2</sup>), and that soil evaporation retrieval is [globally-generally](#) consistent with an independent  
43 estimate from observed soil moisture evolution.

#### 44 1. Introduction

45 Evapotranspiration is an important, yet difficult to estimate (Jasechko et al., 2013), component of the  
46 water cycle, especially in semi-arid lands. Its quantification is crucial for a sustainable management of  
47 scarce water resources. The recent development of remote sensing products and data assimilation  
48 methods have led to a new era in the use of remote sensing data in the various spectral domains to  
49 derive more robust estimates of evapotranspiration at various spatial scales (Crow et al., 2008; Olioso  
50 et al., 2005). Amongst those products, surface temperature provides access to a rough estimate of  
51 water stress. Indeed, moisture limited evapotranspiration triggers an increase in surface temperature  
52 above a theoretical equilibrium value in unstressed conditions (Amano and Salvucci, 1997; Boulet et  
53 al., 2007). Most algorithms based on the use of a remotely sensed surface temperature evaluate a  
54 total latent heat flux corresponding to the sum of the evaporation and the transpiration components:  
55 they're named "single-source models". Total latent heat flux representing the whole surface is  
56 derived as the residual term of the surface energy balance at the time of satellite overpass (Kalma et  
57 al., 2008). Single-source models require a method to relate the temperature at the aerodynamic level  
58 and the surface temperature obtained by remote sensing (Matsushima, 2005). It is very often based  
59 on an additional resistance term or  $kB^{-1}$  (Carlson et al., 1995, Verhoef, 1997) that is heavily  
60 parameterized. Even though the use of single-source models is widespread, dual-source models are  
61 particularly useful because they allow retrieving separate estimates of evaporation and transpiration.  
62 Those components are particularly needed for ecohydrological or agrohydrological applications  
63 (irrigation management, water stress detection...). Moreover, dual-source models provide a more  
64 realistic description of the main water and heat fluxes, even if the vegetation is seen as a single "big  
65 leaf" and the soil a single "big pore" (Kustas et al., 1996). This is especially true for sparse vegetation,  
66 when commonly used scalar profiles within the canopy no longer apply. It also avoids the use of a  
67 parameterized  $kB^{-1}$  (Kustas and Anderson, 2009).

68 Beyond evapotranspiration, estimating water stress is also important to infer the surface water status  
69 and the root zone soil moisture level (Hain et al., 2009). Water stress can be obtained for the surface  
70 as a whole by combining the simulated latent heat flux and the potential latent heat flux, i.e. the  
71 theoretical value of the latent heat in current climatic conditions if the surface was still undergoing  
72 stage one (unstressed) evapotranspiration (Lhomme, 1997). Dual-source energy balance models  
73 allow deriving a rough estimate of the water stress but of the vegetation instead of a soil-vegetation  
74 composite. [They also provide an estimate of the climate-controlled and moisture-limited soil](#)  
75 [evaporation rates.](#) Such frameworks use as input data either the component surface temperatures  
76 (e.g. soil and vegetation components retrieved from directional surface temperature data, Jia et al.,  
77 2003 or Colaizzi et al., 2012) or a single soil-vegetation composite surface skin temperature. For the

78 former, there is no current operational satellite that offers estimates of temperatures at two  
79 contrasted view angles with a very small interval between both acquisitions, even though the soon to  
80 be launched Sentinel-3 mission will have such capability (Donlon et al., 2012). For the latter, the TSEB  
81 model proposes a realistic underlying assumption to downsize the number of unknowns from two  
82 (evaporation E and transpiration T) to one (E or T, Norman et al., 1995). The TSEB model assumes that  
83 in most eco- or agro-systems vegetation has access to enough water in the root zone to transpire at a  
84 potential rate, so that a modeled potential transpiration rate is a valid first guess estimate for T. This  
85 assumption implies that, if vegetation stress is not properly taken into account, the resulting  
86 evaporation will decrease to unrealistic levels (negative fluxes) in order to maintain the same total  
87 surface temperature, so that a retrieved negative evaporation is a good witness of plant water stress.  
88 This assumption is sometimes misleading, and we propose to study its limits.

89 The original version of TSEB (Norman et al., 1995) provides two algorithms to describe the soil-  
90 vegetation-atmosphere interactions, representing respectively the “patch” and the “layer”  
91 approaches following the terminology proposed by Lhomme et al. (2012). In the “layer” approach,  
92 one assumes that the air is well mixed within the canopy space so that air temperature at the  
93 aerodynamic level is rather homogeneous. The vegetation layer completely covers the ground and  
94 prevents the soil from interacting directly (in terms of radiation and turbulent heat transfer) with the  
95 atmospheric reference level: soil and vegetation heat sources are fully coupled through a resistance  
96 network organized in series (Figure 1). In the “patch” approach, soil and canopy sources are located  
97 side by side, and the soil interacts directly with the air above the canopy. There is a possible lateral  
98 gradient in air temperature around the aerodynamic level even though heat transfer around the  
99 canopy is associated to the same momentum transfer: soil and vegetation heat sources are thermally  
100 uncoupled and fluxes are computed with two parallel resistance schemes. In the original TSEB  
101 version, total net radiation is split into soil and vegetation components according to a simple Beer-  
102 Lambert law. Several improvements have been proposed later on and implemented in various TSEB  
103 versions. Amongst them, one can mention the development of a more complex net radiation scheme,  
104 with an initialization of soil and vegetation temperatures in separate formulations of the net radiation  
105 of the soil and the canopy (~~Kustas and Norman, 1999~~) or the use of an incremental decrease of a  
106 transpiration efficiency ~~instead of a bulk retrieval of the latent heat of the vegetation~~ (~~Kustas and~~  
107 ~~Norman, 1999~~; it corresponds roughly to the ratio between the actual and the potential transpiration  
108 rates and matches the definition of the efficiency used in the present work). The TSEB rationale has  
109 been translated into several algorithms, with the possibility of using directional radiative  
110 temperatures (Kustas and Norman, 1997), day-night temperature difference (Guzinski et al., 2013;  
111 Norman et al., 2000), correcting for clumping effects in sparsely vegetated areas (Anderson et al.,  
112 2005), and finally by taking into account a Penman-Monteith formulation for potential transpiration  
113 (Colaizzi et al., 2012).

114 Here, we propose to revisit the “layer/series” and “patch/parallel” formulations in order to build a  
115 new model based on the same rationale that provides the foundation for all TSEB model versions.

116 First, we build on the statement by Colaizzi et al. (2012) that, in semi-arid lands, it is more relevant to  
117 use a ~~classical~~ resistance scheme based on a Penman-Monteith expression instead of the Priestley-  
118 Taylor equation, so that adiabatic exchanges are explicitly described. The most common value of the  
119 Priestley-Taylor coefficient (close to 1.3) has indeed been challenged for natural vegetation and sites



120 with strong vapour pressure deficit values where root zone moisture is not limiting transpiration  
121 (Agam et al., 2010). According to Colaizzi et al. (2014), potential transpiration using Penman-Monteith  
122 equation showed better performances compared to the Priestley-Taylor equation. In particular, these  
123 authors showed a consistent underestimation of T and overestimation of E when using Priestley-  
124 Taylor formulation with the classical 1.3 coefficient, even if total evapotranspiration was similar for  
125 both models.

126 Second, since in the layer approach the vegetation is a semi-infinite cover overlaying the ground, it  
127 appears more consistent that this version of the model takes into account not only the soil-vegetation  
128 interactions of the turbulent fluxes, but also of the radiative fluxes. Conversely, in the patch approach  
129 there is no radiation exchange between the soil and the vegetation patches. This is achieved for the  
130 series model through a multiple reflections description between the soil and the overlaying  
131 vegetation cover in order to stick more closely to the patch and layer representations schematized in  
132 Figure 1.

133 Based on those studies, we propose a generalization of the TSEB model (named SPARSE: Soil Plant  
134 Atmosphere and Remote Sensing Evapotranspiration model) as a linearization of the full set of energy  
135 budget equations and the Choudhury and Monteith (1988) and Shuttleworth and Gurney (1990)  
136 expressions of the aerodynamic resistances. The series model is very close to the soil-plant-  
137 atmosphere interface of the SiSPAT model (Braud et al., 1995). The full set of equations can be solved  
138 either in prescribed conditions (for example, in fully stressed or potential conditions) to compute  
139 transpiration and evaporation rates for given stress levels, or in retrieval mode, identically to TSEB. In  
140 that case, stress levels are deduced from a known (observed) surface temperature. We propose a  
141 third improvement to the existing TSEB model versions, which is similar to what is done in a post-  
142 processing step in the single-source SEBS model (Su, 2002). It consists in bounding each retrieved  
143 individual flux component (T, E) by its corresponding potential level deduced from running the model  
144 in prescribed potential conditions. Indeed, transpiration can be above its potential level when there  
145 is a strong coupling between the soil and the vegetation through conditions at aerodynamic level  
146 (stability correction notably): maximum transpiration for a plant surrounded by very dry bare soil is  
147 increased above the potential transpiration rate as computed in a fully wet environment. This  
148 coupling might be excessive and a potential transpiration of a wet environment is an interesting  
149 baseline to assess excess in this coupling.

150 The main objective of the paper is twofold:

- 151 | 1- To describe the SPARSE model, evaluate it against in-situ data and compare-relate its  
152 | performance with those of the “patch/parallel” and “layer/series” TSEB model formulations,  
153 | with a focus on the potential gain in robustness obtained when limiting evaporation and  
154 | transpiration outputs by their corresponding potential rates derived from SPARSE.
- 155 | 2- Test the retrieval capacities of both “patch/parallel” and “layer/series” versions of the model,  
156 | not only for total evapotranspiration as well as its components (soil evaporation and  
157 | transpiration) but also for water stress, first with synthetic data (simulation experiment) and  
158 | second with in-situ data collected over two wheat fields in semi-arid climate, one irrigated  
159 | and one rainfed. The purpose of the simulation experiment is specifically to test the limits of

160 the underlying first guess assumptions of ~~TSEB and~~ SPARSE, which are identical to those used  
161 in most TSEB versions.

162

## 163 2. Series and parallel versions of the SPARSE model

164

### 165 2.1. SPARSE system of equations

166 The SPARSE model computes the equilibrium surface temperatures of the soil ( $T_s$ ) and the vegetation  
167 ( $T_v$ ) at the meteorological time step as a signature of the energy budget equations of each source.  
168 Five main equations are solved simultaneously. The first two express the continuity (series version) or  
169 the summation (parallel version) of the latent and sensible heat fluxes from the soil and the canopy  
170 to the aerodynamic level and above ~~represent the energy budget of the soil and the vegetation~~, the  
171 third and the fourth represent the energy budget of the soil and the vegetation ~~express the continuity~~  
172 (series version) or the summation (parallel version) of the latent and sensible heat fluxes from the soil  
173 and the canopy to the aerodynamic level and above, and the fifth describes the link between the  
174 radiative surface temperature  $T_{rad}$  and its two component temperature sources (soil  $T_s$  and vegetation  
175  $T_v$ ).

Mis en forme : Anglais (États-Unis)

176 Two versions are derived, which can be regarded as fully coupled (series) and fully uncoupled  
177 (parallel) soil–vegetation–air exchanges (Figure 1). This corresponds to (respectively) the “layer” and  
178 “patch” approaches described in Lhomme et al. (2012). However, the interpretation of the situations  
179 for which one or the other approach is valid differs between TSEB and Lhomme et al. (2012). In TSEB,  
180 both soil and vegetation patches share a common surface boundary layer (and therefore the same  
181 aerodynamic resistance from the aerodynamic level to the reference level) but the patch  
182 representation allows defining different aerodynamic temperatures at the aerodynamic level over the  
183 soil and the vegetation. As pointed out by Lhomme et al (2012), the patch representation should in  
184 theory only apply to patches large enough to develop different surface boundary layers, e.g. fallow  
185 fields amongst wetter and taller vegetated areas rather than bare soil patches even few meters large.  
186 Here, we keep the TSEB assumption for our parallel version and assume that the wind profile above  
187 the aerodynamic level in the canopy and above the soil surface are identical in both versions. ~~The~~  
188 ~~main difference lies therefore in the lateral gradient in aerodynamic temperature: in the series~~  
189 ~~version, a single aerodynamic temperature is computed, while in the parallel version two different~~  
190 ~~aerodynamic temperatures are computed above the soil and the canopy, allowing a small departure~~  
191 ~~of the temperature profiles above the soil and the canopy level from the standard mean profile.~~

192 The various aerodynamic resistances are computed according to Choudhury and Monteith (1988),  
193 Shuttleworth (1985) and Shuttleworth and Gurney (1990) while the stomatal resistance is modelled  
194 according to Braud et al. (1995) for all environmental control factors except water stress which is  
195 replaced by a transpiration efficiency  $\beta_v$ , and the moisture limited evaporation which is governed by  
196 an evaporation efficiency  $\beta_s$  (Mahfouf and Noilhan, 1991). Definitions of  $\beta_s$  and  $\beta_v$  are given just  
197 below.

#### 198 2.1.1. The series model version

199 In the series model the latent heat flux components for the soil ( $LE_s$ ) and the vegetation ( $LE_v$ ) are  
 200 representative averages for the surface as a whole:

$$201 \quad LE_s = \frac{\rho c_p}{\gamma} \beta_s \frac{e_{sat}(T_s) - e_0}{r_{as}} \quad (1)$$

$$202 \quad LE_v = \frac{\rho c_p}{\gamma} \beta_v \frac{e_{sat}(T_v) - e_0}{r_{vv}} \quad (2)$$

203 where  $\rho c_p$  is the product of air density and specific heat,  $\gamma$  the psychrometric constant,  $r_{as}$  the soil to  
 204 aerodynamic level resistance and  $r_{vv}$  the minimum total resistance for latent heat exchange between  
 205 the vegetation and the aerodynamic level (see Annex A1);  $e_{sat}(T_x)$  is the saturated vapour pressure at  
 206 temperature  $T_x$  (x refers to "s" for soil, "v" for vegetation) and  $e_0$  is the partial pressure of vapour at  
 207 the aerodynamic level;  $T_s$  and  $T_v$  are the soil and the vegetation temperatures respectively.

208 This formulation is different from that of the most common TSEB algorithms which use the Priestley-  
 209 Taylor relationship to derive a first estimate of  $LE_v$ . Efficiencies  $\beta_x$  are functionally equivalent to  
 210 surface resistances (again, x referring "s" for soil, "v" for vegetation and is left blank for the total  
 211 evapotranspiration flux). Their range of validity is [0, 1]: if  $\beta_x=1$  then the vegetation transpires at  
 212 potential rate, and if  $\beta_s=1$  the soil evaporation rate is that of a saturated surface, while  $\beta_x=0$  or  $\beta_s=0$   
 213 correspond to a non-transpiring or a non-evaporating surface, respectively. Scaling between those  
 214 extremes depends on the soil moisture content around the root zone (for  $\beta_s$ ) or in the top few  
 215 centimetres (for  $\beta_v$ ). Here,  $r_{vv}/\beta_v$  represents a total canopy resistance including stomatal processes  
 216 while  $r_{as}/\beta_s$  corresponds to a total soil evaporation resistance, both in actual conditions. There is no  
 217 minimum resistance to vapour extraction from the soil porous medium, therefore resistances above  
 218 the soil are the same for sensible and latent heat transfers.

219 In order to reduce the computational cost of solving the system for all unknown variables including  $T_s$   
 220 and  $T_v$ , all non-linear expressions are linearized through Taylor expansion around air temperature so  
 221 that the model can be solved through a simple matrix inversion. This is a requirement if one wants to  
 222 run the model for a large number of pixels. **A non-linear model version using optimization routines of  
 223 the commercial software Matlab™ has been implemented to check the relevance of the linearization,  
 224 but its computational cost is of course much higher.** Eqs. 1 and 2 are converted to Eqs. 3 and 4:

$$225 \quad LE_s \approx \frac{\rho c_p}{\gamma} \beta_s \frac{e_{sat}(T_a) + \Delta(T_s - T_a) - e_0}{r_{as}} \quad (3)$$

$$226 \quad LE_v \approx \frac{\rho c_p}{\gamma} \beta_v \frac{e_{sat}(T_a) + \Delta(T_v - T_a) - e_0}{r_{vv}} \quad (4)$$

227 where  $\Delta$  is the slope of the saturation vapour curve at air temperature  $T_a$ .

228 The only non-linear term that is kept in either version is the dependence of the aerodynamic  
 229 resistance to the stability correction. The latter depends on the difference between the aerodynamic  
 230 temperature and the reference air temperature (Richardson number, cf. Annex A1). Aerodynamic  
 231 temperature is updated iteratively until convergence.

232 According to the layer representation in Figure 1, total fluxes (net radiation, sensible heat flux, latent  
 233 heat flux, soil heat flux) are computed as the sum of the soil and vegetation components. The  
 234 continuity of the latent heat flux below and above the aerodynamic level implies:

235  $LE = LE_s + LE_v = \frac{\rho c_p}{\gamma} \frac{e_0 - e_a}{r_a}$  (5)

236 where  $LE_s$  is expressed in (3) and  $LE_v$  in (4).

237 Continuity of the sensible heat reads:

238  $H = H_s + H_v = \rho c_p \frac{T_0 - T_a}{r_a}$  (6)

239 where  $T_0$  is the aerodynamic temperature and

240  $H_s = \rho c_p \frac{T_s - T_0}{r_{as}}$  (7)

241  $H_v = \rho c_p \frac{T_v - T_0}{r_{av}}$  (8)

242 ( $r_a$  and  $r_{av}$  are the aerodynamic level to reference level and vegetation to aerodynamic level  
243 aerodynamic resistances, resp., see Annex A1 for their complete expression)

244 Net radiation depends on the greybody emissions of the soil and vegetation surfaces at temperature  
245  $T_s$  and  $T_v$ . Taylor expansion for those emission terms in the net radiation estimates leads to:

246  $\sigma T_x^4 \approx \sigma T_a^4 + \rho c_p \frac{4\sigma T_a^3}{\rho c_p} (T_x - T_a) = \sigma T_a^4 + \rho c_p \frac{T_x - T_a}{r_{rad}}$  (9)

247 where  $\sigma$  is the Stefan-Boltzman constant and  $r_{rad}$  represents a "radiative resistance".

248 Net radiation is computed according to the radiative transfer scheme of Merlin and Chehbouni  
249 (2004) which takes into account the multiple reflections between the soil and the vegetation layer in  
250 the shortwave and the longwave domains. Application of Eq. 9 on the various equations of this  
251 scheme leads to a forcing term depending on the incoming shortwave and longwave radiations,  $A_x$ ,  
252 and a linear expression of the unknown surface temperatures  $T_s$  and  $T_v$  divided by the appropriate  
253 radiative resistances  $r_{radx}$  (for the expression of those terms, see Annex A2). For the soil, this leads to:

254  $R_{ns} = A_{ss} - \rho c_p \frac{T_s - T_a}{r_{radss}} - \rho c_p \frac{T_v - T_a}{r_{radsv}}$  (10)

255 and for the canopy:

256  $R_{nv} = A_{vv} - \rho c_p \frac{T_s - T_a}{r_{radvs}} - \rho c_p \frac{T_v - T_a}{r_{radvv}}$  (11)

257 The total flux is:

258  $R_n = R_{ns} + R_{nv}$  (12)

259 The soil heat flux  $G$  is a fraction  $\xi$  of the net radiation available for the whole the soil surface  
260 ( $G = \xi R_{ns}$ ). If the model is run at the same time of the day, for instance with surface temperatures  
261 acquired with a sun-synchronous satellite,  $\xi$  depends mostly on the bare soil fraction cover. For  
262 diurnal variations of  $G$ , a time-dependent expression (e.g. Santanello and Friedl, 2003) should be  
263 preferred.

264 The resulting energy balance for the soil ( $R_{ns} - G = H_s + LE_s$ ) and the canopy ( $R_{nv} = H_v + LE_v$ ) for  
265 the series model can be written as follows:

266  $(1 - \xi)A_{ss} = (1 - \xi)\rho c_p \frac{T_s - T_a}{r_{radss}} + (1 - \xi)\rho c_p \frac{T_v - T_a}{r_{radsv}} + \rho c_p \frac{T_s - T_0}{r_{as}} + \frac{\rho c_p}{\gamma} \beta_s \frac{e_{sat}(T_a) + \Delta(T_s - T_a) - e_0}{r_{as}}$  (13)

267 for the soil and

$$268 \quad A_{vv} = \rho c_p \frac{T_s - T_a}{r_{radvs}} + \rho c_p \frac{T_v - T_a}{r_{radvv}} + \rho c_p \frac{T_v - T_0}{r_{av}} + \frac{\rho c_p}{\gamma} \beta_v \frac{e_{sat}(T_a) + \Delta(T_v - T_a) - e_0}{r_{vv}} \quad (14)$$

269 for the vegetation.

270 Finally, the link between the radiative surface temperature  $T_{rad}$  and the net longwave radiation  
271 components is:

$$272 \quad \sigma T_{rad}^4 = R_{atm} - R_{an} \quad (15)$$

273 where  $R_{atm}$  is the incoming atmospheric radiation and  $R_{an}$  is the net longwave radiation of the whole  
274 surface, which depends on  $T_s$  and  $T_v$  and can be expressed as follows:

$$275 \quad R_{an} = A_{atm} - \rho c_p \left( \frac{1}{r_{radss}} + \frac{1}{r_{radvs}} \right) (T_s - T_a) - \rho c_p \left( \frac{1}{r_{radvv}} + \frac{1}{r_{radsv}} \right) (T_v - T_a) \quad (16)$$

276 The forcing term for the net longwave radiation  $A_{atm}$  is given in Annex A2.

277 The equation relating the radiative surface temperature  $T_{rad}$  and the surface temperatures  $T_s$  and  $T_v$   
278 is thus:

$$279 \quad \sigma T_{rad}^4 + A_{atm} - R_{atm} = \rho c_p \left( \frac{1}{r_{radss}} + \frac{1}{r_{radvs}} \right) (T_s - T_a) + \rho c_p \left( \frac{1}{r_{radvv}} + \frac{1}{r_{radsv}} \right) (T_v - T_a) \quad (17)$$

280

### 281 **2.1.2. The parallel model version**

282

283 For the parallel model, all fluxes are representative of each patch (Figure 1). The total resistance is the  
284 sum of the aerodynamic resistance  $r_a$  and the surface resistances  $r_{as}$  (for the soil) or  $r_{vv}$  (for the  
285 canopy). The transpiration rate of the vegetated subpixel (in W/m<sup>2</sup>) is thus:

$$286 \quad LE_v = \frac{\rho c_p}{\gamma} \beta_v \frac{e_{sat}(T_v) - e_a}{r_{vv} + r_a} \quad (18)$$

287 while for the separate patch of bare soil the evaporation rate is:

$$288 \quad LE_s = \frac{\rho c_p}{\gamma} \beta_s \frac{e_{sat}(T_s) - e_a}{r_{as} + r_a} \quad (19)$$

289 After linearization, we have:

$$290 \quad LE_s \approx \frac{\rho c_p}{\gamma} \beta_s \frac{D_a + \Delta(T_s - T_a)}{r_{as} + r_a} \quad (20)$$

$$291 \quad LE_v \approx \frac{\rho c_p}{\gamma} \beta_v \frac{D_a + \Delta(T_v - T_a)}{r_{vv} + r_a} \quad (21)$$

292 where  $D_a = e_{sat}(T_a) - e_a$  is the vapour pressure deficit at reference level.

293 For the parallel model, the sensible heat flux rate above each patch is:

$$294 \quad H_s = \rho c_p \frac{T_s - T_a}{r_{as} + r_a} \quad (22)$$

295 for the soil, and

296  $H_v = \rho c_p \frac{T_v - T_a}{r_{av} + r_a}$  (23)

297 for the vegetation.

298 The value of the Leaf Area Index used for the parallel model is a “clump LAI” obtained by dividing the  
 299 total LAI by the fraction cover of the vegetation  $f_c$  (Lhomme and Chehbouni, 1999). Total fluxes are  
 300 the sum of the soil and vegetation components also weighted by their relative contribution,  $f_c$  for the  
 301 vegetation and  $1-f_c$  for the soil:

302  $LE = (1 - f_c)LE_s + f_c LE_v$  (24)

303 where  $LE_s$  is expressed according to (20) and  $LE_v$  to (21), and

304  $H = (1 - f_c)H_s + f_c H_v$  (25)

305 where  $H_s$  is expressed according to (22) and  $H_v$  to (23).

306 The stability correction for the aerodynamic resistance  $r_a$  depends on an average aerodynamic  
 307 temperature computed from the total sensible heat flux  $H$ :

308  $T_0 = T_a + \frac{H r_a}{\rho c_p}$

309 (26) For the parallel model, the sensible heat flux rate and the related continuity of the flux through  
 310 the aerodynamic level above each patch leads to the following equations:

311  $H_s = \rho c_p \frac{T_s - T_a}{r_{as} + r_a} = \rho c_p \frac{T_s - T_{0s}}{r_{as}}$  (22)

312 for the soil, and

313  $H_v = \rho c_p \frac{T_v - T_a}{r_{av} + r_a} = \rho c_p \frac{T_v - T_{0v}}{r_{av}}$  (23)

314 for the vegetation, where  $T_{0s}$  is the aerodynamic temperature above the soil and  $T_{0v}$  is the  
 315 aerodynamic temperature above the canopy.

316  
 317 In the parallel model, fluxes from the soil and the vegetation components are computed  
 318 independently except again for the stability correction for the transfer resistance between the  
 319 aerodynamic level and the reference level, which depends on an average aerodynamic temperature  
 320 computed as a weighted average of  $T_{0s}$  and  $T_{0v}$ :

321  $T_{0a} = (1 - f_c)T_{0s} + f_c T_{0v}$  (24)

322 Values of  $T_{0s}$  and  $T_{0v}$  can be derived from (22) and (23) once  $T_s$  and  $T_v$  are known. The value of the  
 323 Leaf Area Index used for the parallel model is a “clump LAI” obtained by dividing the total LAI by the  
 324 fraction cover of the vegetation  $f_c$  (Lhomme and Chehbouni, 1999). Total fluxes are the sum of the soil  
 325 and vegetation components also weighted by their relative contribution,  $f_c$  for the vegetation and  $1-f_c$   
 326 for the soil:

327  $LE_a = (1 - f_c)LE_{s_a} + f_c LE_{v_a}$  (25)

328 where  $LE_{s_a}$  is expressed according to (20) and  $LE_{v_a}$  to (21), and

Mis en forme : Anglais (États-Unis)

Mis en forme : Anglais (États-Unis)

Mis en forme : Anglais (États-Unis)

Mis en forme : Anglais (États-Unis)

Mis en forme : Anglais (États-Unis)

Mis en forme : Anglais (États-Unis)

Mis en forme : Anglais (États-Unis)

Mis en forme : Anglais (États-Unis)

Mis en forme : Anglais (États-Unis)

Mis en forme : Anglais (États-Unis)

Mis en forme : Anglais (États-Unis)

Mis en forme : Anglais (États-Unis)

Mis en forme : Anglais (États-Unis)

Mis en forme : Anglais (États-Unis)

Mis en forme : Anglais (États-Unis)

Mis en forme : Anglais (États-Unis)

Mis en forme : Anglais (États-Unis)

Mis en forme : Anglais (États-Unis)

Mis en forme : Anglais (États-Unis)

Mis en forme : Anglais (États-Unis)

Mis en forme : Anglais (États-Unis)

Mis en forme : Anglais (États-Unis)

329  $H_a = (1 - f_e)H_s + f_e H_{va}$  (26)

330 where  $H_s$  is expressed according to (22) and  $H_v$  to (23).

331  
 332 For the parallel model, incoming solar and atmospheric radiations are fully available for each source.  
 333 The net radiation components are solved independently and, like the turbulent fluxes, summed  
 334 according to their respective cover fraction. The radiative transfer scheme is simpler than for the  
 335 series model. The Taylor expansion of the net radiation expression for the soil writes:

336  $R_{ns} = A_s - \rho c_p \frac{T_s - T_a}{r_{rads}}$  (27)

337 and for the vegetation:

338  $R_{nv} = A_v - \rho c_p \frac{T_v - T_a}{r_{radv}}$  (28)

339 where  $A_s$  and  $A_v$  are the radiation forcing terms for the soil and the vegetation, respectively (See  
 340 Annex A2 for their numerical expression).

341 The total flux is:

342  $R_n = (1 - f_c)R_{ns} + f_c R_{nv}$  (29)

343 The soil heat flux  $G$  is a fraction  $\xi$  of the net radiation available on the bare soil patch ( $G =$   
 344  $(1 - f_c) \xi R_{ns}$ ).

345 Finally, the respective energy balance equations for the soil and the vegetation patches of the  
 346 parallel model are:

347  $(1 - \xi)A_s = (1 - \xi)\rho c_p \frac{T_s - T_a}{r_{rads}} + \rho c_p \frac{T_s - T_a}{r_{as} + r_a} + \frac{\rho c_p}{\gamma} \beta_s \frac{D_a + \Delta(T_s - T_a)}{r_{as} + r_a}$  (30)

348 and

349  $A_v = \rho c_p \frac{T_v - T_a}{r_{radv}} + \rho c_p \frac{T_v - T_a}{r_{av} + r_a} + \frac{\rho c_p}{\gamma} \beta_v \frac{D_a + \Delta(T_v - T_a)}{r_{vv} + r_a}$  (31)

350 For the parallel version, the net longwave radiation has also a simpler expression than for the series  
 351 model:

352  $R_{an} = (1 - f_c) \left[ \varepsilon_s (R_{atm} - \sigma T_a^4) - \rho c_p \frac{T_s - T_a}{r_{rads}} \right] + f_c \left[ \varepsilon_v (R_{atm} - \sigma T_a^4) - \rho c_p \frac{T_v - T_a}{r_{radv}} \right]$  (32)

353 The equation relating the radiative surface temperature  $T_{rad}$  and the surface temperatures  $T_s$  and  $T_v$   
 354 is thus:

355  $\sigma T_{rad}^4 - R_{atm} + [(1 - f_c)\varepsilon_s + f_c \varepsilon_v] [R_{atm} - \sigma T_a^4] = (1 - f_c)\rho c_p \frac{T_s - T_a}{r_{rads}} + f_c \rho c_p \frac{T_v - T_a}{r_{radv}}$  (33)

356

357 **2.2. "Prescribed" and "retrieval" modes**

358 The system of five equations to be solved simultaneously consists in Eqs. 5, 6, 13, 14 and 17 for the  
 359 series model, and Eqs. 2524, 2625, 30, 31 and 33 for the parallel model. This system can be solved in

- Mis en forme : Anglais (États-Unis)
- Mis en forme : Anglais (États-Unis)
- Mis en forme : Anglais (États-Unis)
- Mis en forme : Anglais (États-Unis)
- Mis en forme : Anglais (États-Unis)

360 a forward mode for which the surface temperature is an output, and an inverse mode when the  
361 surface temperature is an input. The SPARSE model combines both modes (cf. Figure 2).

362 If the soil and the vegetation efficiencies are known (for example through an ancillary two  
363 compartments water budget model) then the model is run in a forward mode from prescribed water  
364 stress conditions (from fully stressed to potential). In that case the system is solved for the following  
365 unknowns:  $T_{rad}$ ,  $T_s$ ,  $T_w$ ,  $e_0$  and  $T_0$ .  $T_{rad}$  in this prescribed mode is then an output of the system  
366 computed from Eqs. 17 and 33 after solving for  $T_s$ ,  $T_w$ ,  $e_0$  and  $T_0$  in the other four equations. This mode  
367 has two direct applications. It can be used independently from the retrieval mode to generate an  
368 equilibrium surface temperature at the time of the satellite overpass in order to assimilate surface  
369 temperature measurements from known  $\beta_s$  and  $\beta_v$  values computed at the daily or subdaily timesteps  
370 from a hydrological model (e.g. Er-raki et al., 2008). It is also implemented as a final step in the  
371 retrieval mode to provide theoretical limits corresponding to maximum reachable levels of sensible  
372 heat (fully stressed conditions) or latent heat (potential conditions) for each component (the soil and  
373 the vegetation). Output fluxes from the retrieval run are bounded by those limiting cases. In full  
374 potential conditions,  $\beta_s=\beta_v=1$  while in fully stressed conditions  $\beta_s=\beta_v=0$ .

375 In retrieval conditions (inverse mode),  $T_{rad}$  is known and is derived from satellite observations or in-  
376 situ measurements in the thermal infra red domain. In order to compute the various fluxes of the  
377 energy balance, the full set of five equations must be solved simultaneously by inverting ~~the~~ the  
378 same matrix corresponding to Eqs. 5, 6, 13, 14 and 17 for the series model and Eqs. 2524, 2625, 30,  
379 31 and 33 for the parallel model. In that case however, contrarily to the prescribed mode, the  
380 problem is initially ill-posed since the system contains six unknowns: evaporation  $LE_s$  and  
381 transpiration  $LE_v$ , surface temperature components  $T_s$  and  $T_w$  and aerodynamic level conditions  $e_0$   
382 and  $T_0$ .  $LE_s$  and  $LE_v$  values are directly converted into stress levels  $\beta_s$  and  $\beta_v$  using Eqs. 3 and 4 (series  
383 model) or 20 and 21 (parallel model). In order to downsize the number of unknowns, SPARSE carries  
384 out the same rationale than the TSEB model: as a first guess, the vegetation is supposed to transpire  
385 at potential rate, therefore  $\beta_v$  is set to 1, and the system is solved for unknown  $LE_s$  (thus  $\beta_s$ ),  $T_s$ ,  $T_w$ ,  $e_0$   
386 and  $T_0$ . If a negative  $LE_s$  is obtained, then the assumption of an unstressed canopy proves to be  
387 inconsistent with the observed surface temperature level. In that case, one assumes that the  
388 vegetation is suffering from water stress. This means that root zone soil moisture is depleted under  
389 critical levels, and that, most probably, the soil surface is already long dry. Therefore,  $\beta_s$  is set to 0 and  
390 the system is solved for  $LE_v$  (thus  $\beta_v$ ) instead of  $LE_s$ . Finally, if  $LE_v$  is negative, fully stressed conditions  
391 are imposed for both the soil and the vegetation independently from  $T_{rad}$ . Of course, inconsistent  
392 positive values of  $LE_s$  corresponding to slightly stressed vegetation conditions can occur when one  
393 assumes that the vegetation is unstressed, but in that case the model won't be able to detect this  
394 inconsistency. The limit of this hypothesis will be assessed in Section 3 through a synthetic case  
395 study.

396 Finally, in order to ensure that  $LE_x$  outputs are within realistic bounds,  $LE_x$  values obtained by running  
397 SPARSE in "retrieval" conditions are limited by the evapotranspiration components in potential  
398 conditions  $LE_x(\beta_s=1, \beta_v=1)$  computed by SPARSE in prescribed potential conditions (Figure2). This  
399 procedure is the dual source equivalent of what is done in in a similar way to the single-source model  
400 SEBS (Su, 2002). For consistency, if  $LE_x$  is limited by  $LE_x(\beta_s=1, \beta_v=1)$ , all fluxes of the corresponding  
401 component energy balance ( $Rn_x, H_x$  and  $G$ ) are set to their values obtained by the "prescribed" mode

Mis en forme : Police :Italique

Mis en forme : Police :Italique

Mis en forme : Police :Italique



402 | in potential conditions, i.e.  $Rn_x(\beta_s=1, \beta_v=1)$ ,  $H_x(\beta_s=1, \beta_v=1)$  and  $G(\beta_s=1, \beta_v=1)$ . The impact of limiting  
403  $LE_x$  outputs on the model performance will be assessed in Section 4.

404 Also, an arbitrary minimum positive value of  $LE_s = 30 \text{ W/m}^2$  is used as the threshold for vegetation  
405 stress detection instead of 0, in order to take into account the contribution of vapour transfer from  
406 within the topsoil porous network (Boulet et al., 1997).

407

### 408 **3. Assessing the retrieval properties of SPARSE through a synthetic case study**

409

#### 410 **3.1. Principles of the simulation experiment**

411 The strong underlying assumptions behind SPARSE are (i) in a first guess the vegetation is supposed to  
412 be unstressed, and (ii) water stress of the vegetation is always concomitant to a non evaporative soil.  
413 This simplification of the soil-vegetation-atmosphere continuum impacts not only the total  
414 evapotranspiration retrieval but also its resulting partition between transpiration and soil  
415 evaporation. It is thus important to assess the limits of both assumptions. To do so, a synthetic  
416 simulation experiment is proposed.

417 The rationale of the synthetic test is as follows: for each combination of known water stress levels  
418 affecting either the transpiration or the evaporation of the soil, one can simulate through the energy  
419 budgets of the soil and the vegetation the resulting component temperatures  $T_s$  and  $T_v$  and the  
420 surface temperature of the whole surface (synthetic  $T_{rad}$ ). If one assumes that the satellite is actually  
421 measuring this temperature, it can be used as input data to get back to the soil evaporation and  
422 transpiration levels and their corresponding efficiencies through the retrieval mode. If there was a  
423 unique bijective relationship between the component temperatures and the temperature of the  
424 whole surface, the retrieved stress levels would correspond to the exact combination of the stress  
425 levels used to generate the synthetic  $T_{rad}$ . Of course this is not the case and many different  
426 combinations of soil and vegetation efficiency values will correspond to the same equilibrium surface  
427 temperature. However, one expects that the whole surface energy balance is well constrained by the  
428 knowledge of  $T_{rad}$ , i.e. that each value of  $T_{rad}$  corresponds to only one surface stress level (or total  
429 efficiency). In other words, we expect that SPARSE will not always partition accurately total ET in E  
430 and T, but will retrieve the ET value relatively satisfactorily.

431 The objective of the synthetic stress is to assess the inconsistencies of the decision tree that  
432 distributes acceptable stress values between the soil and the vegetation, as well as its impact on the  
433 component and total evapotranspiration retrieval performances.

434

#### 435 **3.2. Set-up of the synthetic test**

436 In this simulation experiment, the SPARSE model is run sequentially in its two operating modes: the  
437 “prescribed” or “forward” mode to generate an estimate of the radiative surface temperature from  
438 prescribed  $\beta_s$  and  $\beta_v$  efficiencies, and the “retrieval” or “inverse” mode to retrieve  $\beta_s$  and  $\beta_v$   
439 efficiencies using as input data the surface temperature obtained previously through the “prescribed”  
440 mode (“synthetic test” branch of Figure 2). The test consists therefore in computing a mixed surface  
441 radiative temperature ( $T_{rad}$ ), soil evaporation ( $LE_s$ ), transpiration ( $LE_v$ ) and evapotranspiration ( $LE$ ) for

442 each possible combination of soil evaporation ( $\beta_s \in [0,1]$ ) and transpiration ( $\beta_v \in [0,1]$ ) efficiencies  
443 in 0.1 increments with the SPARSE model in prescribed mode, then forcing the SPARSE model with  
444  $T_{rad}$  to retrieve new  $LE_s$ ,  $LE_v$  and total evapotranspiration  $LE$  values as well as the corresponding  
445 efficiencies ( $\beta_s$ ,  $\beta_v$  and  $\beta$  for the total).  $\beta$  is deduced as the ratio between two total evapotranspiration  
446 estimates: one with actual  $\beta_s$  and  $\beta_v$  and one with  $\beta_s=\beta_v=1$ . In order to assess the limits of the model  
447 assumptions for each version, the prescribed and the retrieval modes are run for the same version  
448 (series or parallel): the surface temperature obtained by each combination of  $\beta_s$  and  $\beta_v$  for the series  
449 model (resp. the parallel model) in prescribed conditions is used as input for the series model in  
450 retrieval mode (resp. the parallel model). The retrieval performance is then assessed by comparing  
451 these new retrieved  $\beta_s$ ,  $\beta_v$  and  $\beta$  values and the ones used to generate  $T_{rad}$ . If the retrieval is fully  
452 consistent, those efficiencies must match. The test is carried out for average dry climate conditions  
453 ( $R_g=800 \text{ W/m}^2$ ,  $RH=50\%$ ,  $u_a=2\text{m/s}$ ,  $T_a=25^\circ\text{C}$ ) and a Leaf Area Index characteristic of maximum  
454 development stage of a cereal cover in dry climates ( $LAI=3$ ).

455

### 456 3.3. Results

457 Results for the total evapotranspiration efficiency retrieval are illustrated in Figure 3. One expects  
458 rather good performances (albeit some bias) close to the first guess assumptions (transpiration close  
459 to potential conditions, i.e.  $\beta_v \cong 1$  and low soil evaporation i.e.  $\beta_s \cong 0$ ) with a degradation when soil  
460 evaporation is high and transpiration is low. In Figure 3, retrieved total efficiency is compared to the  
461 prescribed total efficiency for various incremental values of  $\beta_v$  for two discrete levels of  $\beta_s$  (0.6 and  
462 0.2, top plots), and for incremental values of  $\beta_s$  for two discrete levels of  $\beta_v$  (0.8 and 0.4, bottom  
463 plots).

464 Total evapotranspiration and its corresponding  $\beta$  efficiency value is well retrieved for each [ $\beta_s$ ,  $\beta_v$ ]  
465 combination for the series model formulation (blue points all aligned along the [1:1] line), while for  
466 the parallel model  $\beta$  is reasonably well retrieved for situations close to the model assumptions, i.e. a  
467 low  $\beta_s$  and a high  $\beta_v$ . For extreme stress values when the assumption underlying SPARSE algorithms is  
468 challenged (low transpiration and non negligible soil evaporation) the parallel model tends to  
469 overestimate  $\beta$ .

470 In Figure 4, the performance of transpiration (top plots) and evaporation (bottom plots) efficiency  
471 retrievals are assessed separately. Since the first guess of SPARSE is that the vegetation is unstressed,  
472 the model will tend to overestimate  $\beta_v$ . This is the case for all transpiration efficiency values, with, as  
473 expected, a larger difference close to a fully transpiring canopy when the inconsistency in  $\beta_s$  retrieval  
474 is not yet detected. Indeed, for  $\beta_v$  values close to 1, the initial guess of an unstressed canopy leads to  
475 assign a fix value of 1 to  $\beta_v$ . The vegetation temperature is therefore underestimated, and the soil  
476 temperature that matches the total surface radiative temperature is overestimated. In turn, sensible  
477 heat over the soil is overestimated, the soil net radiation is underestimated, and the resulting soil  
478 evaporation computed as a residual term is underestimated. As long as this underestimation does not  
479 lead to a negative value of  $\beta_s$ , the model does not detect the discrepancy. Consequently, especially  
480 for a wet soil (top plot on the left hand side,  $\beta_s = 0.86$ ),  $\beta_v$  retrievals match poorly the prescribed  
481 values, and  $\beta_v$  values cling to the unstressed boundary, except for very high prescribed stress levels  
482 ( $\beta_v$  below 0.4 for the series model, 0.2 for the parallel one).

483 Despite this overestimation,  $\beta_s$  retrievals are relatively consistent if the soil is very dry (top plot on the  
484 right hand side,  $\beta_s = 0.2$ ). Once again  $\beta_s$  retrievals by the series model are closer to the prescribed  
485 values than those of the parallel model. Conversely, soil evaporation retrievals (bottom plots) show,  
486 as expected, a slight underestimation when the vegetation is close to unstressed (left hand plot,  $\beta_v$   
487  $= 0.8$ ). Its amplitude is fairly constant and mirrors the overestimation of the transpiration efficiencies  
488 when the soil is dry. In that case, blue dots (series) and red squares (parallel) of the retrievals are  
489 close to the [1:1] line for all  $\beta_s$  levels.

490 For conditions far from the initial assumption, e.g. low transpiration efficiencies, soil evaporation is  
491 largely underestimated. One must note that this is the case for both models and all  $\beta_s$  values. Again,  
492 moderately stressed vegetation and a low level soil evaporation rate will always be interpreted in  
493 terms of composite surface temperature as a dry soil and fully transpiring vegetation. As a  
494 consequence, very small rain events on an otherwise dry soil will most probably be interpreted as a  
495 dry soil surface with slightly stressed vegetation. Those cases, not very frequent but not rare either,  
496 must be treated with care in a data assimilation perspective.

497 All those biases should be kept in mind when interpreting results from all dual-source models based  
498 on the same rationale: the fact that the total flux is well simulated does not always means that the  
499 component fluxes are consistent, let alone realistic. This has been shown for this particular synthetic  
500 dataset.

501 This test has been carried out using SPARSE due to the possibility the model offers to combine both  
502 modes in a consistent synthetic experiment. Its outcomes are illustrated for this model and a single  
503 set of vegetation and climatic conditions. We don't claim that the differences between series and  
504 parallel retrieval capacities also fully apply to TSEB but since they share the same strong underlying  
505 assumptions and differ mostly by their parameterization of the fluxes, we're convinced that similar  
506 differences would be found with TSEB if TSEB could be run in a prescribed mode.

507

#### 508 4. Application over irrigated and rainfed wheat

509

##### 510 4.1. Datasets

511 Two datasets were used to assess the performance of the series and parallel versions of the  
512 SPARSE model over a whole growing season. The first experimental dataset was collected over a  
513 rainfed wheat with green Leaf Area Index values up to 2 and the second over an irrigated wheat with  
514 green LAI up to 4. Both have been grown in a semi-arid climate (central Tunisia and Morocco). Surface  
515 temperature data were acquired with ~~an~~ a nadir-looking Apogee thermoradiometer, while energy  
516 fluxes were measured according to classical FLUXNET recommendations (Baldocchi et al., 2001) with  
517 Campbell™ CSAT sonic anemometers and Krypton fast response hygrometers. Observed and  
518 simulated latent heat flux values (half hourly averages in  $W/m^2$ ) are compared at midday (local  
519 standard time) in all sky conditions. For the rainfed wheat site, there was clearly a problem with the  
520 fast response psychrometer with an energy balance closure of 60 %. Thus for that site the closure was  
521 forced and the corrected LE was computed as  $R_n - H - G$ . For the irrigated site, the half hourly closure  
522 was of the order of 80%. For this site closure was achieved with the conservation of the Bowen ratio  
523  $H/LE$ , thus the corrected LE was computed as  $(R_n - G)/(1 + H/LE)$ . ~~Bowen ratio and the residual method~~

Mis en forme : Retrait : Première  
ligne : 0.85 cm

524 | ~~have been used to close the energy balance for the irrigated and rainfed wheat sites, respectively,~~  
525 | ~~due to the fast response hygrometer failures of the latter site.~~ Data for the irrigated wheat site have  
526 | been acquired during the 2004 growing season (B124 site, Boulet et al., 2012), while the experiment  
527 | for the rainfed wheat took place in 2012.

528 | Leaf Area Index was estimated with hemispherical photography every 2 to 3 weeks depending on the  
529 | phenological cycle, validated by destructive measurements during key stages (growth and full cover).  
530 | Vegetation height was measured at the same dates. Temporal interpolation of Leaf Area Index for  
531 | both sites is shown in Figure 5.

532

#### 533 | 4.2. Evapotranspiration estimates

534 | Two sets of **SPARSE** simulations are derived for each model version (series or parallel): in the set the  
535 | most faithful to the original TSEB, outputs are not limited by potential heat flux values; in the second  
536 | set, outputs are, like in SEBS, bounded by the potential and fully stressed flux rates considered at  
537 | absolute maximum and minimum reachable values for evaporation as well as transpiration, whatever  
538 | the “oasis” or micro-advection heat transfer might be. Again, this is legitimate for the parallel version,  
539 | but for the series version one must inquire if local advection effects do not enhance latent heat flux  
540 | values over the total potential value of a uniformly wet surface. No calibration is performed, the  
541 | minimum stomatal resistance value is arbitrarily set to a realistic level for herbaceous vegetation (100  
542 | s/m, [Gentine et al., 2007](#)) and the  $G/Rn_s$  ratio  $\xi$  is set to 40% (value often encountered around  
543 | midday for bare soils in arid climates). This is consistent with the potential use of this model which is  
544 | designed to estimate ET routinely from remote sensing data, based on surface properties derived per  
545 | land use type in a similar way to most SVATs applied to continental scales. Those values are of course  
546 | less sensitive than the uncertainty on the input variable  $T_{rad}$  (not shown). In order to relate those first  
547 | guess results to those obtained by the series and parallel Kustas et al. (1999) TSEB versions, TSEB is  
548 | also applied with a default value for the Priestley-Taylor coefficient (1.26).

549 | Total flux values are shown in Figures 6 and 7 for the bounded sets and RMSE values for both  
550 | bounded and unbounded sets are reported in Table 1. In both cases (series and parallel versions) the  
551 | RMSE values are of similar order of magnitudealmost similar and consistent with values found in the  
552 | literature (cf. Li et al., 2005). The bounded series outputs display the best performances, with RMSE  
553 | values lowered by 4 to more than 10 W/m<sup>2</sup>. Without bounding, values of evaporation and  
554 | transpiration above potential levels are obtained for the series version during vegetation growth, and  
555 | some negative values of transpiration are found during late maturity and beginning of senescence.  
556 | -RMSE values for the parallel TSEB version of Kustas et al. (1999) are very close to that of the SPARSE  
557 | parallel version while RMSE values for the TSEB series model ~~built from Cammalleri et al. (2010)~~ are  
558 | similar to the RMSE values displayed by both parallel versions.

559 | Retrieval performances of the other energy balance components in the bounded case have also been  
560 | assessed. Statistics are shown in Table 2. The series model shows slightly better retrieval  
561 | performances for soil heat flux for both sites, but only for net radiation for the irrigated wheat and for  
562 | sensible heat for the rainfed wheat site. This is consistent with Li et al. (2005) and Morillas et al.  
563 | (2013) who showed that the series TSEB version was more robust than the parallel version, also their  
564 | relative performances were close.

565

### 566 4.3. Water stress estimates

567 Low RMSE values for the total latent heat flux do not warranty that total water stress is correctly  
568 simulated. Indeed, if moisture availability in the root zone is large enough to maintain ET at potential  
569 levels, the prescribed model in potential conditions can already explain a very large amount of the  
570 information content within the observed time series, and the added value of TIR data might be  
571 limited. It is thus important to assess the amount of information introduced by the surface  
572 temperature itself, i.e. information on moisture limited evaporation and transpiration rates (i.e.  
573 second stage evaporation, cf. Boulet et al., 2004). Water stress is usually defined as the  
574 complementary part to 1 of the ratio between the actual and the potential evapotranspiration rates.  
575 It is expected to scale between 0 (unstressed surface) and 1 (fully stressed surface). Retrieved and  
576 observed surface water stress values have been estimated from potential evapotranspiration rates  
577 generated with the SPARSE model in prescribed conditions ( $\beta_s = \beta_v = 1$ ). Simulated and observed water  
578 stress values are computed as  $1 - LE/LE_p$  and  $1 - LE_{obs}/LE_p$  respectively, where  $LE_{obs}$  is the instantaneous  
579 observed latent heat flux while  $LE$  and  $LE_p$  are the simulated latent heat flux in actual and potential  
580 conditions respectively. Total stress is thus functionally equivalent to  $1 - \beta$ . Results are shown in Figure  
581 8 and 9. As expected, surface stress is much higher for the rainfed than for the irrigated wheat field.  
582 The scatter is quite large, therefore showing the intrinsic limit of stress retrieval from naturally noisy  
583 TIR data as already pointed out by numerous studies (Gentine et al., 2010; Katul et al., 1998;  
584 Lagouarde et al., 2013, 2015). However, broad tendencies are well reproduced, with most points  
585 located within a confidence interval of 0.2 indicated by dotted lines along the 1:1 line. This is  
586 encouraging in a data assimilation perspective. One must also note that it includes small  $LE$  and  $LE_p$   
587 values for which measurement uncertainty can be as large as the flux itself. To scale those stress  
588 values back to potential evapotranspiration, the  $LE_p$  order of magnitude is indicated as marker size in  
589 Figure 8 and 9. Most outliers have smaller  $LE_p$  values while the points with the largest  $LE_p$  fall within  
590 the space delimited by the two dotted lines of the confidence interval.

591 Some points with little to no evaporation attest the difficulty to represent accurately the  
592 conditions close to the potential levels and might be related to the theoretical limit of the model for  
593 small vegetation stress values illustrated in figure 3, especially at low evaporation efficiencies.

594

### 595 4.4. Soil evaporation efficiency

596 As shown in the previous sections as well as many previous studies on soil-vegetation-atmosphere  
597 interactions in the literature (Li et al., 2005; Morillas et al., 2013), series and parallel versions have  
598 fairly similar performances in total flux retrieval even though the series version shows slightly better  
599 values for the selected statistical criterion. However, as illustrated with the synthetic case, it might  
600 not be the case for component flux retrieval. In order to check the consistency of component flux  
601 retrieval, one needs a measurement of either soil evaporation or transpiration. In neither sites  
602 transpiration data have been collected: measuring transpiration for a cereal cover is quite  
603 challenging. On the other hand, surface soil moisture data (at a depth of around 5 cm) are available at  
604 both sites. Of course, soil moisture at 5 cm does not always react to small rainfall events, but it is a  
605 good driver of soil evaporation despite its influence by shallow roots.

606 We therefore decided to compare the retrieved soil evaporation efficiency to a fairly independent  
607 evaluation noted  $\beta_{s,e}$  derived from the observed time series of soil moisture in the top 5 cm ( $\theta_{0-5cm}$ )  
608 instead of using TIR data. We used the efficiency model of Merlin et al. (2011) to derive  $\beta_{s,e}$ :

$$609 \quad \beta_{s,e} = \left[ 0.5 - 0.5 \cos \left( \pi \frac{\theta_{0-5cm}}{\theta_{sat}} \right) \right]^p \quad (34)$$

610 | Where  $\theta_{sat}$  is the [in-situ](#) water content at saturation ([0.30 for the rainfed site and 0.48 for the irrigated](#)  
611 [wheat](#)) and  $p$  is fixed to 1 for the loamy site (rainfed wheat) and 0.5 for the clay site (irrigated wheat)  
612 according to  $1-LE/LE_p$  observations at the beginning and the end of the growing season when the soil  
613 is almost bare.

614 Since the surface temperature (and thus the partition between  $LE_s$  and  $LE_v$ ) reacts immediately to  
615 atmospheric turbulence (Lagouarde et al., 2015) or very small rainfall events,  $\beta_s$  instantaneous  
616 retrievals by SPARSE show larger fluctuations than  $\beta_{s,e}$ . Indeed, the latter reacts mostly to the largest  
617 rainfall events (wetting of the entire 5 cm topsoil). Meteorological forcing can vary quickly and impact  
618 the potential soil evaporation rate  $LE_{sp}$ , but the latter is less sensitive to turbulence than  $T_{rad}$ . In order  
619 to smooth out the quick fluctuations of  $\beta_s$  retrievals by SPARSE, we compare 5 days running averages  
620 of  $\beta_s$  and  $\beta_{s,e}$ .

621 The resulting  $\beta_s$  and  $\beta_{s,e}$  evaporation efficiencies are shown on Figure 10 (rainfed wheat) and 11  
622 (irrigated wheat). For both sites, increasing and decreasing trends of  $\beta_s$  and  $\beta_{s,e}$  are mostly  
623 synchronous, although their amplitude varies throughout the growing season. Due to irrigation,  $\beta_s$   
624 values are on average higher for the irrigated than the rainfed wheat site.

625 For the rainfed site, both models simulate fairly large values of  $\beta_s$  compared to  $\beta_{s,e}$  at the beginning of  
626 the season. The parallel model agrees well with  $\beta_{s,e}$  towards the end of the growing stage (DOY 30-  
627 70) while the series model matches very closely  $\beta_{s,e}$  at maximum cover and early senescence  
628 (reduction of  $\beta_s$  from DOY 70 to DOY 100). Both models agree well with  $\beta_{s,e}$  at the end of the season  
629 (DOY 120-170) except for the last ten days. The small rainfall event around DOY 125 is not sufficient  
630 to impact  $\beta_{s,e}$  but affects  $\beta_s$  in both model versions, whereas the soil moisture increase around DOY  
631 105 is mostly missed out by either version.

632 For the irrigated wheat, soil evaporation is mostly in the energy limited stage for the first half of the  
633 observation period, and  $\beta_s$  remains close to 1. This is due to the complement irrigation up to the  
634 middle of the maturation phase. The magnitude of both drying events around DOY 40 and DOY 100 is  
635 very well retrieved by the series model and somewhat less by the parallel model. Again,  $\beta_s$  reacts  
636 more strongly to the small rainfall event around DOY90 than what is indicated from soil moisture.

637 At the very end of the season both model versions differ greatly from the  $\beta_{s,e}$  estimates and remain  
638 close to the potential rate for both sites.

## 639 **5. Discussion and conclusion**

640 A new model based on the TSEB rationale, SPARSE, has been presented. Innovation lies mostly in the  
641 formulation of the energy balance equations and the use of complementary modes (prescribed and  
642 retrieval) which allow to bound the outputs by realistic limiting flux values which ensure increased  
643 robustness. We demonstrated with two datasets that using bounding relationships based on  
644 potential conditions decreases the Root Mean Square Error by up to 11 W/m<sup>2</sup> from values of the

645 order of 50-80 W/m<sup>2</sup>. Theoretical limitations of the performance of the evapotranspiration  
646 components (evaporation and transpiration) retrievals from a single radiative surface temperature  
647 have been inferred over rainfed and irrigated wheat fields at seasonal scales, as well as through a  
648 theoretical simulation exercise. For very high vegetation stress levels According to results obtained in  
649 Section 3, it is almost impossible to retrieve a non-zero soil evaporation at medium to large LAI values  
650 for very high vegetation stress levels. Also, and by construction, transpiration tends to be  
651 overestimated in most ranges but specifically when only slightly stressed. Within these limits, the  
652 SPARSE model shows good retrieval performances of evapotranspiration compared to the original  
653 TSEB. This comparison must be treated with special care since both models are run with no prior  
654 calibration of the poorly known parameters such as the minimum stomatal resistance (for SPARSE) or  
655 the Priestly-Taylor coefficient (for TSEB). If a value of  $r_{stmin}=50$  s/m is used, a value also reported for  
656 wheat crops in more temperate regions, RMSE on latent heat flux increases by 4 W/m<sup>2</sup> in bounded  
657 conditions for the rainfed wheat site (62 W/m<sup>2</sup>) and 13 W/m<sup>2</sup> for the irrigated wheat site (66 W/m<sup>2</sup>)  
658 for the series version. For the parallel model it increases by 12 W/m<sup>2</sup> (82 W/m<sup>2</sup>) and 8 W/m<sup>2</sup> (74  
659 W/m<sup>2</sup>), respectively.

660 As expected for cereal covers whose homogeneity is usually well represented by a “layer” approach,  
661 the series version provides in general better estimates in both real and synthetic cases tested. Those  
662 cases are representative of cereals typically grown in semi-arid lands in irrigated and non-irrigated  
663 areas. Both models should be tested for other conditions of heterogeneity (sparse crops, orchards,  
664 row crops) whose geometrical features are closer to the “patch” description.

665 Estimates of water stress have also been looked at. Water stress is an interesting variable that can be  
666 assimilated in all hydrological or SVAT models in order to compute moisture-limited  
667 evapotranspiration rates. Even if the points in the simulated vs observed scatterplots have a  
668 significant number of outliers, i.e. points outside the 0.4-2 range along the 1:1 line in Figures 8 and 9,  
669 the results indicate that the information retrieved from TIR data is useful in a data-assimilation  
670 perspective since the broad tendencies are well reproduced.

671 Estimates of soil evaporation efficiency have been evaluated against a reconstructed time series  
672 relying on observed soil moisture at the soil surface and therefore independent from any surface  
673 temperature measurement. This reconstruction is of course model-dependent (Merlin et al., 2011 in  
674 our case) and must be considered with care, but despite this we found that both efficiency values are  
675 consistent, except at the beginning and the end of the season, partly due to very small rainfall events,  
676 but also probably to the poor understanding of turbulence processes over low or senescent  
677 vegetation. It seems that the transpiration of the quasi-senescent vegetation encountered at this  
678 period of the year is not always well simulated by the model even if total and green LAI values seem  
679 realistic. This could be related to the change in soil-vegetation radiation exchange and drag partition  
680 in a drying vegetation with shrinking leaves and standing straw. In order to smooth out the scale  
681 differences between the information provided by soil moisture (a time-continuous variable) and that  
682 of surface temperature (influenced by high frequency turbulent fluctuations) we compared 5 days  
683 moving averages. This is consistent with the potential data assimilation method of  $\beta$  or  $LE$  estimated  
684 from TIR data that one could use in a SVAT model for example: a smoother is more likely to  
685 outperform a sequential assimilation algorithm for short observation windows since the former will  
686 naturally smooth-out the high order fluctuations due to high order fluctuations of  $T_{rad}$ . Simpler  
687 models would perhaps provide similar performances of soil evaporation efficiencies, for instance in

Mis en forme : Exosant

Mis en forme : Exosant

Mis en forme : Exosant

Mis en forme : Exosant

Mis en forme : Exosant

Mis en forme : Exosant

688 rainfed agriculture where surface soil moisture is well constrained by rainfall, but in irrigated areas it  
689 is interesting to get proper timing of water inputs and this can be achieved with relatively good  
690 confidence with this model provided that TIR information is available frequently enough.

691 Future work will assess the potential use of microwave data (radar) to infer topsoil moisture and  
692 constraint the inversion procedure using a first guess efficiency value generated from topsoil moisture  
693 estimates. Current work is directed towards assessing the model performance over other crops,  
694 including orchards, and other climates.

695 [SPARSE needs more input data than TSEB, for instance relative humidity. The impact of uncertainty on](#)  
696 [available meteorological data \(reanalysis or remote-sensing meteorological products vs local](#)  
697 [meteorological stations network\) on SPARSE model performance will also be assessed in the future.](#)

## 698 **References**

699 Agam, N., Kustas, W. P., Anderson, M. C., Norman, J. M., Colaizzi, P. D., Howell, T. A., Prueger, J. H.,  
700 Meyers, T. P., and Wilson, T. B.: Application of the Priestley-Taylor Approach in a Two-Source Surface  
701 Energy Balance Model, *Journal of Hydrometeorology*, 11, 185-198, 10.1175/2009jhm1124.1, 2010.

702 Amano, E., and Salvucci, G. D.: Detection of three signatures of soil-limited evaporation, *Remote*  
703 *Sensing of Environment*, 67, 108-122, 1997.

704 Anderson, M. C., Norman, J. M., Kustas, W. P., Li, F., Prueger, J. H., and Mecikalski, J. R.: Effects of  
705 Vegetation Clumping on Two-Source Model Estimates of Surface Energy Fluxes from an Agricultural  
706 Landscape during SMACEX, *Journal of Hydrometeorology*, 6, 892-909, 10.1175/jhm465.1, 2005.

707 Baldocchi, D., Falge, E., Gu, L., Olson, R., Hollinger, D., Running, S., Anthoni, P., Bernhofer, C., Davis, K.,  
708 Evans, R., Fuentes, J., Goldstein, A., Katul, G., Law, B., Lee, X., Malhi, Y., Meyers, T., Munger, W.,  
709 Oechel, W., Paw, K. T., Pilegaard, K., Schmid, H. P., Valentini, R., Verma, S., Vesala, T., Wilson, K., and  
710 Wofsy, S.: FLUXNET: A New Tool to Study the Temporal and Spatial Variability of Ecosystem-Scale  
711 Carbon Dioxide, Water Vapor, and Energy Flux Densities, *Bulletin of the American Meteorological*  
712 *Society*, 82, 2415-2434, 10.1175/1520-0477(2001)082<2415:fantts>2.3.co;2, 2001.

713 Boulet, G., Braud, I., and Vauclin, M.: Study of the mechanisms of evaporation under arid conditions  
714 using a detailed model of the soil-atmosphere continuum. Application to the EFEDA I experiment,  
715 *Journal of Hydrology*, 193, 114-141, 1997.

716 Boulet, G., Chehbouni, A., Braud, I., Duchemin, B., and Lakhel, A.: Evaluation of a two-stage  
717 evaporation approximation for contrasting vegetation cover, *Water Resources Research*, 40,  
718 W1250710.1029/2004wr003212, 2004.

719 Boulet, G., Chehbouni, A., Gentine, P., Duchemin, B., Ezzahar, J., and Hadria, R.: Monitoring water  
720 stress using time series of observed to unstressed surface temperature difference, *Agricultural and*  
721 *Forest Meteorology*, 146, 159-172, 10.1016/j.agrformet.2007.05.012, 2007.

722 Boulet, G., Olioso, A., Ceschia, E., Marloie, O., Coudert, B., Rivalland, V., Chirouze, J., and Chehbouni,  
723 G.: An empirical expression to relate aerodynamic and surface temperatures for use within single-



- 724 source energy balance models, *Agricultural and Forest Meteorology*, 161, 148-155,  
725 10.1016/j.agrformet.2012.03.008, 2012.
- 726 Braud, I., Dantas-Antonino, A. C., Vauclin, M., Thony, J. L. and Ruelle, P.: A Simple Soil-Plant-  
727 Atmosphere Transfer model (SiSPAT), development and field verification, *Journal of Hydrology*, 166,  
728 231-260, 1995.
- 729 ~~Cammalleri, C., Anderson, M. C., Ciraolo, G., D'Urso, G., Kustas, W. P., La Loggia, G., and Minacapilli,  
730 M.: The impact of in-canopy wind profile formulations on heat flux estimation in an open orchard  
731 using the remote sensing based two source model, *Hydrology and Earth System Sciences*, 14, 2643-  
732 2659, 10.5194/hess-14-2643-2010, 2010.~~
- 733 Carlson, T. N., Taconet, O., Vidal, A., Gilles, R. R., Olioso, A., and Humes, K.: An overview of the  
734 workshop on thermal remote-sensing held at La-Londe-Les-Maures, France, September 20-24, 1993.,  
735 *Agricultural and Forest Meteorology*, 77, 141-151, 1995.
- 736 Choudhury, B. J., and Monteith, J. L.: A 4-layer model for heat-budget of homogeneous land surfaces,  
737 *Quarterly Journal of the Royal Meteorological Society*, 114, 373-398, 10.1002/qj.49711448006, 1988.
- 738 Colaizzi, P. D., Kustas, W. P., Anderson, M. C., Agam, N., Tolck, J. A., Evett, S. R., Howell, T. A., Gowda, P.  
739 H., and O'Shaughnessy, S. A.: Two-source energy balance model estimates of evapotranspiration  
740 using component and composite surface temperatures, *Advances in Water Resources*, 50, 134-151,  
741 10.1016/j.advwatres.2012.06.004, 2012.
- 742 Colaizzi, P. D., Agam, N., Tolck, J. A., Evett, S. R., Howell, T. A., Gowda, P. H., O'Shaughnessy, S. A.,  
743 Kustas, W. P., and Anderson, M. C.: Two-source energy balance model to calculate E, T and ET:  
744 comparison of Priestley-Taylor and Penman-Monteith formulations and two time scaling methods,  
745 *Transactions of the Asabe*, 57, 479-498, 2014.
- 746 Crow, W. T., Kustas, W. P., and Prueger, J. H.: Monitoring root-zone soil moisture through the  
747 assimilation of a thermal remote sensing-based soil moisture proxy into a water balance model,  
748 *Remote Sensing of Environment*, 112, 1268-1281, 2008.
- 749 ~~Donlon, C., Berruti, B., Buongiorno, A., Ferreira, M.-H., Féménias, P., Frerick, J., Goryl, P., Klein, U.,  
750 Laur, H., Mavrocordatos, C., Nieke, J., Rebhan, H., Seitz, B., Stroede, J., and Sciarra, R.: The global  
751 monitoring for environment and security (GMES) sentinel-3 mission, *Remote Sens. Environ.*, 120, 37-  
752 57, 2012.~~
- 753 Er-Raki, S., Chehbouni, A., Hoedjes, J., Ezzahar, J., Duchemin, B., and Jacob, F.: Improvement of FAO-  
754 56 method for olive orchards through sequential assimilation of Thermal infrared based estimates of  
755 ET, *Agricultural Water Management*, 95, 309-321, 2008.
- 756 ~~Gentine, P., Entekhabi, D., Chehbouni, A., Boulet, G., Duchemin, B., : Analysis of evaporative fraction  
757 diurnal behaviour. *Agricultural and Forest Meteorology*, 143(1-2): 13-29, 2007.~~
- 758 Gentine, P., Entekhabi, D., and Polcher, J.: Spectral Behaviour of a Coupled Land-Surface and  
759 Boundary-Layer System, *Boundary-Layer Meteorology*, 134, 157-180, 10.1007/s10546-009-9433-z,  
760 2010.

Mis en forme : Anglais (États-Unis)

Mis en forme : Anglais (États-Unis)

761 Guzinski, R., Anderson, M. C., Kustas, W. P., Nieto, H., and Sandholt, I.: Using a thermal-based two  
762 source energy balance model with time-differencing to estimate surface energy fluxes with day-night  
763 MODIS observations, *Hydrology and Earth System Sciences*, 17, 2809-2825, 10.5194/hess-17-2809-  
764 2013, 2013.

765 Hain, C. R., Mecikalski, J. R., and Anderson, M. C.: Retrieval of an Available Water-Based Soil Moisture  
766 Proxy from Thermal Infrared Remote Sensing. Part I: Methodology and Validation, *Journal of*  
767 *Hydrometeorology*, 10, 665-683, 10.1175/2008jhm1024.1, 2009.

768 Jasechko, S., Sharp, Z. D., Gibson, J. J., Birks, S. J., Yi, Y., and Fawcett, P. J.: Terrestrial water fluxes  
769 dominated by transpiration, *Nature*, 496, 347-350, 10.1038/nature11983,  
770 [http://www.nature.com/nature/journal/v496/n7445/abs/nature11983.html#supplementary-](http://www.nature.com/nature/journal/v496/n7445/abs/nature11983.html#supplementary-information)  
771 [information](http://www.nature.com/nature/journal/v496/n7445/abs/nature11983.html#supplementary-information), 2013.

772 Jia, L., Su, Z. B., van den Hurk, B., Menenti, M., Moene, A., De Bruin, H. A. R., Yrisarry, J. J. B., Ibanez,  
773 M., and Cuesta, A.: Estimation of sensible heat flux using the Surface Energy Balance System (SEBS)  
774 and ATSR measurements, *Physics and Chemistry of the Earth*, 28, 75-88, 10.1016/s1474-  
775 7065(03)00009-3, 2003.

776 Kalma, J. D., McVicar, T. R., and McCabe, M. F.: Estimating Land Surface Evaporation: A Review of  
777 Methods Using Remotely Sensed Surface Temperature Data, *Surveys in Geophysics*, 29, 421-469,  
778 10.1007/s10712-008-9037-z, 2008.

779 Katul, G. G., Schieldge, J., Hsieh, C. I., and Vidakovic, B.: Skin temperature perturbations induced by  
780 surface layer turbulence above a grass surface, *Water Resources Research*, 34, 1265-1274,  
781 10.1029/98wr00293, 1998.

782 Kustas, W., and Anderson, M.: Advances in thermal infrared remote sensing for land surface  
783 modeling, *Agricultural and Forest Meteorology*, 149, 2071-2081, 10.1016/j.agrformet.2009.05.016,  
784 2009.

785 Kustas, W. P., Humes, K. S., Norman, J. M., and Moran, M. S.: Single- and Dual-Source Modeling of  
786 Surface Energy Fluxes with Radiometric Surface Temperature, *Journal of Applied Meteorology*, 35,  
787 110-121, 10.1175/1520-0450(1996)035<0110:sadsmo>2.0.co;2, 1996.

788 Kustas, W. P., and Norman, J. M.: A two-source approach for estimating turbulent fluxes using  
789 multiple angle thermal infrared observations, *Water Resources Research*, 33, 1495-1508,  
790 10.1029/97wr00704, 1997.

791 Kustas, W. P., and Norman, J. M.: Evaluation of soil and vegetation heat flux predictions using a simple  
792 two-source model with radiometric temperatures for partial canopy cover, *Agricultural and Forest*  
793 *Meteorology*, 94, 13-29, 10.1016/s0168-1923(99)00005-2, 1999.

794 Lagouarde, J.-P., Bach, M., Sobrino, J. A., Boulet, G., Briottet, X., Cherchali, S., Coudert, B., Dadou, I.,  
795 Dedieu, G., Gamet, P., Hagolle, O., Jacob, F., Nerry, F., Olioso, A., Ottlé, C., Roujean, J.-l., and Fargant,  
796 G.: The MISTIGRI thermal infrared project: scientific objectives and mission specifications,  
797 *International Journal of Remote Sensing*, 34, 3437-3466, 10.1080/01431161.2012.716921, 2013.

798 Lagouarde, J.-P., Irvine, M., and Dupont, S.: atmospheric turbulence induced errors on measurements  
799 of surface temperature from space, *Remote Sens. Environ.*, 168,40-53, doi:10.1016/j.rse.2015.06.018,  
800 2015

801 Lhomme, J. P.: Towards a rational definition of potential evaporation, *Hydrology and Earth System  
802 Sciences*, 1, 257-264, 1997.

803 Lhomme, J.P., and Chehbouni, A.: Comments on dual-source vegetation-atmosphere transfer models.  
804 *Agricultural and Forest Meteorology*, 94, 269–273, 1999.

805 Lhomme, J. P., Montes, C., Jacob, F., and Prevo, L.: Evaporation from Heterogeneous and Sparse  
806 Canopies: On the Formulations Related to Multi-Source Representations, *Boundary-Layer  
807 Meteorology*, 144, 243-262, 10.1007/s10546-012-9713-x, 2012.

808 Li, F. Q., Kustas, W. P., Prueger, J. H., Neale, C. M. U., and Jackson, T. J.: Utility of remote sensing-based  
809 two-source energy balance model under low- and high-vegetation cover conditions, *Journal of  
810 Hydrometeorology*, 6, 878-891, 2005.

811 Mahfouf, J., and Noilhan, J.: Comparative study of various formulations of evaporations from bare soil  
812 using in situ data, *Journal of Applied Meteorology*, 30, 1354-1365, 1991.

813 Matsushima, D.: Relations between aerodynamic parameters of heat transfer and thermal-infrared  
814 thermometry in the bulk surface formulation, *Journal of the Meteorological Society of Japan*, 83, 373-  
815 389, 2005.

816 Merlin, O., and Chehbouni, A.: Different approaches in estimating heat flux using dual angle  
817 observations of radiative surface temperature, *International Journal of Remote Sensing*, 25, 275-289,  
818 10.1080/0143116031000116408, 2004.

819 Merlin, O., Al Bitar, A., Rivalland, V., Beziat, P., Ceschia, E., and Dedieu, G.: An Analytical Model of  
820 Evaporation Efficiency for Unsaturated Soil Surfaces with an Arbitrary Thickness, *Journal of Applied  
821 Meteorology and Climatology*, 50, 457-471, 10.1175/2010jamc2418.1, 2011.

822 Morillas, L., Garcia, M., Nieto, H., Villagarcia, L., Sandholt, I., Gonzalez-Dugo, M. P., Zarco-Tejada, P. J.,  
823 and Domingo, F.: Using radiometric surface temperature for surface energy flux estimation in  
824 Mediterranean drylands from a two-source perspective, *Remote Sensing of Environment*, 136, 234-  
825 246, 10.1016/j.rse.2013.05.010, 2013.

826 Norman, J. M., Kustas, W. P., and Humes, K. S.: Source approach for estimating soil and vegetation  
827 energy fluxes in observations of directional radiometric surface temperature, *Agricultural and Forest  
828 Meteorology*, 77, 263-293, 1995.

829 Norman, J. M., Kustas, W. P., Prueger, J. H., and Diak, G. R.: Surface flux estimation using radiometric  
830 temperature: A dual-temperature-difference method to minimize measurement errors, *Water  
831 Resources Research*, 36, 2263-2274, 2000.

- 832 Olioso, A., Inoue, Y., Ortega-Farias, S., Demarty, J., Wigneron, J. P., Braud, I., Jacob, F., Lecharpentier,  
833 P., Otlí, C., Calvet, J. C., and Brisson, N.: Future directions for advanced evapotranspiration modeling:  
834 Assimilation of remote sensing data into crop simulation models and SVAT models, *Irrigation and*  
835 *Drainage Systems*, 19, 377-412, 2005.
- 836 Santanello, J. A., and Friedl, M. A.: Diurnal covariation in soil heat flux and net radiation, *Journal of*  
837 *Applied Meteorology*, 42, 851–862, doi:10.1175/1520-0450(2003)042<0851:dcishf>2.0.co;2, 2003.
- 838 Shuttleworth, W. J., and Gurney, R. J.: The theoretical relationship between foliage temperature and  
839 canopy resistance in sparse crops, *Quarterly Journal of the Royal Meteorological Society*, 116, 497-519,  
840 10.1002/qj.49711649213, 1990.
- 841 Shuttleworth, W. J., and Wallace, J.S.: Evaporation from sparse crops - an energy combination theory,  
842 *Quarterly Journal of the Royal Meteorological Society*, 111, 839-855, 1985.
- 843 Su, Z.: The Surface Energy Balance System (SEBS) for estimation of turbulent heat fluxes, *Hydrology*  
844 *and Earth System Sciences*, 6, 85-99, 2002.
- 845 Verhoef, A., de Bruin, H. A. R., and van den Hurk, B. J. J. M.: Some Practical Notes on the Parameter  
846  $k_B-1$  for Sparse Vegetation, *Journal of Applied Meteorology*, 36, 560-572, 1997.

847

#### 848 **Acknowledgements**

849 This work was mostly supported by the French Space Agency (CNES) through TOSCA projects EVA2IRT  
850 and EVASPA3. Financial support by ANR for the TRANSMED project AMETHYST (ANR-12-TMED-0006-  
851 01) and PHC Maghreb for the project N° 32592VE (“Estimation spatialisée de l'utilisation de l'eau par  
852 l'agriculture pluviale et irriguée au Maghreb”) are also gratefully acknowledged. Sustained financial  
853 and in kind support by IRD and the MISTRALS (Mediterranean Integrated Studies at Regional And  
854 Local Scales) program through its SICMED component is also acknowledged. The authors extend their  
855 thanks to the technical teams of IRD, INAT, CTV-Chebika and INGC for their strong collaboration and  
856 support for the implementation of ground-truth measurements.

857

858 **Annex A1:** Expression of the various resistances according to Shuttleworth and Gurney (1990)

$$r_a = \frac{\ln\left(\frac{z-d}{z_{om}}\right)^2}{k^2 u_a (1 + Ri)^m}$$

$$r_{as} = \frac{z_v e^{n_{sw}} \ln\left(\frac{z-d}{z_{om}}\right) \left( e^{\frac{-n_{sw} z_{om,s}}{z_v}} - e^{\frac{-n_{sw}(d+z_{om})}{z_v}} \right)}{n_{sw} k^2 u_a (z_v - d)^{0.5}}$$

$$r_{av} = \left( \frac{w}{u_a} \frac{\ln\left(\frac{z-d}{z_{om}}\right)}{\ln\left(\frac{z_v-d}{z_{om}}\right)} \right) \frac{n_{sw}}{4\alpha_0 LAI (1 - e^{-0.5n_{sw}})}$$

$$r_{vv} = r_{av} + \frac{r_{stmin} \Pi f}{LAI_g LAI}$$

859 Where  $u_o$  is the wind speed measured at height  $z$ ,  $z_v$  the vegetation height,  $d$  the displacement  
860 height,  $z_{om}$  the roughness length for momentum exchange,  $n_{sw}=2.5$ ,  $w$  the width of the leaves (in  
861 cm),  $\alpha_o=0.005$ ,  $r_{stmin}$  the minimum stomatal resistance and  $z_{om,s}=0.005m$  is the roughness length for  
862 momentum exchange over bare soil.  $Ri = \frac{5g(z-d)(T_o-T_a)}{T_a u_o^2}$  is the stability correction (Richardson  
863 number);  $m=0.75$  in unstable conditions and  $m=2$  in stable conditions.  $\Pi f$  represent the product of  
864 weighting stress functions related to environmental factors affecting the stomatal resistance  
865 (temperature, solar radiation, vapour pressure deficit) and are taken from Braud et al. (1995). The  
866 rule of thumb applies:  $z_{om}=0.13*z_v$  and  $d=0.66*z_v$ .  
867

Mis en forme : Indice

Mis en forme : Indice

Mis en forme : Indice

868 **Annex A2:** Forcing terms and radiative resistances of the net radiation model for the series and the  
869 parallel versions of SPARSE.

870 For the series version:

$$871 A_{ss} = (a_{rads} + b_{rads})\sigma T_a^4 + c_{rads}$$

$$872 r_{radss} = -\frac{\rho c_p}{4\sigma T_a^3 a_{rads}}$$

$$873 r_{radsv} = -\frac{\rho c_p}{b_{rads} 4\sigma T_a^3}$$

$$874 A_{vv} = (a_{radv} + b_{radv})\sigma T_a^4 + c_{radv}$$

$$875 r_{radvs} = -\frac{\rho c_p}{a_{radv} 4\sigma T_a^3}$$

$$876 r_{radvv} = -\frac{\rho c_p}{b_{radv} 4\sigma T_a^3}$$

$$877 A_{atm} = (a_{rads} + b_{rads} + a_{radv} + b_{radv})\sigma T_a^4 + c_{ratms} + c_{ratmv}$$

878 where

$$a_{rads} = -\frac{\varepsilon_s [(1-f_c) + \varepsilon_v f_c]}{1-f_c(1-\varepsilon_s)(1-\varepsilon_v)}$$

$$b_{rads} = a_{radv} = \frac{\varepsilon_v \varepsilon_s f_c}{1-f_c(1-\varepsilon_s)(1-\varepsilon_v)}$$

$$c_{ratms} = \frac{(1-f_c)\varepsilon_s R_{atm}}{1-f_c(1-\varepsilon_s)(1-\varepsilon_v)}$$

$$c_{rads} = \frac{R_g(1-\alpha_s)(1-f_c)}{1-f_c\alpha_s\alpha_v} + c_{ratms}$$

$$b_{radv} = -f_c \varepsilon_v \left[ 1 + \frac{\varepsilon_s + (1-f_c)(1-\varepsilon_s)}{1-f_c(1-\varepsilon_s)(1-\varepsilon_v)} \right]$$

$$c_{ratmv} = f_c \varepsilon_v R_{atm} \left[ 1 + \frac{(1-f_c)(1-\varepsilon_s)}{1-f_c(1-\varepsilon_s)(1-\varepsilon_v)} \right]$$

$$879 c_{radv} = R_g(1-\alpha_v)f_c \left[ 1 + \frac{\alpha_s(1-f_c)}{1-f_c\alpha_s\alpha_v} \right] + c_{ratmv}$$

880  $(\alpha_s$  and  $\varepsilon_s$  are the albedo and the emissivity of the soil,  $\alpha_v$  and  $\varepsilon_v$  are the albedo and the emissivity of  
 881 the canopy, and  $R_g$  is the global incoming radiation,  $f_c = 1 - e^{-0.5LAI/\cos\varphi}$  where the view zenith  
 882 angle  $\varphi=0^\circ$  for both datasets;  $R_{atm} = 1.24(e_a/T_a)^{1/7}\sigma T_a^4$

Mis en forme : Justifié

Mis en forme : Police : Symbol

Mis en forme : Police : (Par défaut)  
+ Corps

883 For the parallel version:

884  $A_s = (1 - \alpha_s)R_g + \varepsilon_s(R_{atm} - \sigma T_a^4)$

885  $A_v = (1 - \alpha_v)R_g + \varepsilon_v(R_{atm} - \sigma T_a^4)$

886  $r_{rads} = \frac{\rho c_p}{4\varepsilon_s\sigma T_a^3}$


887  $r_{radv} = \frac{\rho c_p}{4\varepsilon_v\sigma T_a^3}$

888

889 **Annex A3 : Symbols**

$a_{rads}$	Coefficient in $r_{rads}$ , $A_{atm}$ and $A_{ss}$
$a_{radv}$	Coefficient in $r_{radv}$ , $A_{atm}$ and $A_{vv}$
$A_s$	Forcing term of the soil net radiation for the parallel model ( $W m^{-2}$ )
$A_v$	Forcing term of the vegetation net radiation for the parallel model ( $W m^{-2}$ )
$A_{ss}$	Forcing term of the soil net radiation for the series model ( $W m^{-2}$ )
$A_{vv}$	Forcing term of the vegetation net radiation for the series model ( $W m^{-2}$ )
$b_{rads}$	Coefficient in $r_{rads}$ , $A_{atm}$ and $A_{ss}$
$b_{radv}$	Coefficient in $r_{radv}$ , $A_{atm}$ and $A_{vv}$
$c_p$	Specific heat of air at constant pressure ( $J kg^{-1} K^{-1}$ )
$c_{rads}$	Coefficient in $A_{ss}$
$c_{radv}$	Coefficient in $A_{vv}$
$c_{ratms}$	Coefficient in $A_{atm}$
$c_{ratmv}$	Coefficient in $A_{atm}$
$d$	Displacement height (m)
$e_a$	Air vapour pressure at reference level (Pa)
$e_o$	Air vapour pressure at the aerodynamic level (Pa)
$e_{sat}(T_x)$	Saturated vapour pressure at temperature $T_x$ (Pa)
$f_c$	Vegetation cover fraction
$G$	Soil heat flux ( $W m^{-2}$ )
$g$	Gravitational constant ( $m s^{-2}$ )
$H$	Total sensible heat flux ( $W m^{-2}$ )
$H_s$	Sensible heat flux from the soil ( $W m^{-2}$ )
$H_v$	Sensible heat flux from the canopy ( $W m^{-2}$ )
<u>LAI</u>	<u>Total Leaf Area Index</u>
<u>LAI<sub>g</sub></u>	<u>Green Leaf Area Index</u>
$LE$	Total latent heat flux ( $W m^{-2}$ )
$LE_p$	Total latent heat flux in potential conditions ( $W m^{-2}$ )
$LE_s$	Latent heat flux from the soil ( $W m^{-2}$ )
$LE_{sp}$	Latent heat flux from the soil in potential conditions ( $W m^{-2}$ )
$LE_v$	Latent heat flux from the canopy ( $W m^{-2}$ )
$LE_{vp}$	Latent heat flux from the canopy in potential conditions ( $W m^{-2}$ )
$m$	Coefficient of the stability function
$n_{sw}$	Coefficient in $r_{sw}$
$r_a$	Aerodynamic resistance between the aerodynamic level and the reference level ( $s m^{-1}$ )
$R_{an}$	Longwave net radiation ( $W m^{-2}$ )
$r_{as}$	Aerodynamic resistance between the <u>soil aerodynamic level</u> and the <u>aerodynamic level</u> / <u>reference level</u> ( $s m^{-1}$ )

Mis en forme : Indice

$R_{atm}$	Incoming atmospheric radiation ( $W m^{-2}$ )
$r_{av}$	Aerodynamic resistance between the <u>vegetation aerodynamic level</u> and the <u>aerodynamic level reference level</u> ( $s m^{-1}$ )
$R_g$	Incoming solar radiation ( $W m^{-2}$ )
$Ri$	Richardson number
$R_n$	Total net radiation ( $W m^{-2}$ )
$R_{ns}$	Net radiation over the soil ( $W m^{-2}$ )
$R_{nv}$	Net radiation over the canopy ( $W m^{-2}$ )
$r_{rad}$	Radiative resistance ( $s m^{-1}$ )
$r_{rads}$	Soil radiative resistance for the parallel model ( $s m^{-1}$ )
$r_{radv}$	Canopy radiative resistance for the parallel model ( $s m^{-1}$ )
$r_{radss}$	Soil radiative resistance for the soil net radiation in the series model ( $s m^{-1}$ )
$r_{radsv}$	Canopy radiative resistance for the soil net radiation in the series model ( $s m^{-1}$ )
$r_{radvs}$	Soil radiative resistance for the vegetation net radiation in the series model ( $s m^{-1}$ )
$r_{radvv}$	Canopy radiative resistance for the vegetation net radiation in the series model ( $s m^{-1}$ )
$r_{stmin}$	Minimum stomatal resistance ( $s m^{-1}$ )
$r_{sv}$	<del>surface</del> <u>Surface</u> resistance between the aerodynamic level and the reference level ( $s m^{-1}$ )
$T_0$	Aerodynamic temperature (K)
$T_{as}$	<del>Aerodynamic temperature over the soil patch</del> (K)
$T_{av}$	<del>Aerodynamic temperature over the vegetation patch</del> (K)
$T_a$	Air temperature at reference level (K)
$T_{rad}$	<u>Radiative surface temperature</u> (K)
$T_s$	Soil surface temperature (K)
$T_v$	Vegetation surface temperature (K)
$u_a$	Horizontal wind speed at reference level ( $s m^{-1}$ )
$w$	Leaf width (cm)
$z$	<del>Referene</del> <u>Reference</u> height where air forcing variables are measured (m)
$z_{om}$	Roughness height (m)
$z_{oms}$	Equivalent roughness length of the underlying bare soil in absence of vegetation (m)
$z_v$	Vegetation height (m)
$\alpha_0$	Coefficient in $r_{av}$
$\alpha_s$	Soil albedo
$\alpha_v$	Vegetation albedo
$\beta$	Evapotranspiration efficiency
$\beta_s$	Evaporation efficiency
$\beta_{s_e}$	Merlin et al. (2011) evaporation efficiency
$\beta_v$	Transpiration efficiency
$\epsilon_s$	Emissivity of the soil
$\epsilon_v$	Emissivity of the vegetation
$\Delta$	Slope of the vapour pressure deficit at $T_a$ ( $Pa K^{-1}$ )
$\gamma$	Psychrometric constant ( $Pa K^{-1}$ )
$\rho$	Air density ( $kg m^{-3}$ )
$\sigma$	Stefan-Boltzmann constant ( $W m^{-2} K^{-4}$ )
$\theta_{0.5cm}$	Integrated volumetric soil moisture in the top 5 cm
$\theta_{sat}$	Volumetric soil moisture at saturation
	<u>View zenith angle (rad)</u>

890

Mis en forme : Police : (Par défaut)  
+Corps

Mis en forme : Police : (Par défaut)  
+Corps, 10 pt

Mis en forme : Police : 10 pt